Atomic and molecular data for spacecraft re-entry plasmas

2016 Plasma Sources Sci. Technol. 25 033004

(http://iopscience.iop.org/0963-0252/25/3/033004)

IOP Publishing Plasma Sources Science and Technology

Plasma Sources Sci. Technol. **25** (2016) 033004 (27pp) doi:10.1088/0963-0252/25/3/033004

Topical Review

Atomic and molecular data for spacecraft re-entry plasmas

R Celiberto[1,2], I Armenise[2], M Cacciatore[2], M Capitelli[2,3], F Esposito[2], P Gamallo[4], R K Janev[5], A Laganà[6], V Laporta[2,7], A Laricchiuta[2], A Lombardi[6], M Rutigliano[2], R Sayós[4], J Tennyson[7] and J M Wadehra[8]

[1] Dipartimento di Ingegneria Civile, Ambientale, del Territorio, Edile e di Chimica, Politecnico di Bari, Bari, Italy
[2] PLASMI Lab, CNR NANOTEC, Bari, Italy
[3] Dipartimento di Chimica, Università degli Studi di Bari, Bari, Italy
[4] Departament de Química Física and Institut de Química Teòrica i Computacional, Universitat de Barcelona, Barcelona, Spain
[5] Macedonian Academy of Sciences and Arts, Skopje, Macedonia
[6] Dipartimento di Chimica Biologia e Biotecnologie, Università di Perugia, Perugia, Italy
[7] Department of Physics and Astronomy, University College London, London, UK
[8] Department of Physics and Astronomy, Wayne State University, Detroit, MI, USA

E-mail: roberto.celiberto@poliba.it

Received 26 November 2015, revised 22 February 2016
Accepted for publication 21 March 2016
Published 17 May 2016

Abstract

The modeling of atmospheric gas, interacting with the space vehicles in re-entry conditions in planetary exploration missions, requires a large set of scattering data for all those elementary processes occurring in the system. A fundamental aspect of re-entry problems is represented by the strong non-equilibrium conditions met in the atmospheric plasma close to the surface of the thermal shield, where numerous interconnected relaxation processes determine the evolution of the gaseous system towards equilibrium conditions. A central role is played by the vibrational exchanges of energy, so that collisional processes involving vibrationally excited molecules assume a particular importance. In the present paper, theoretical calculations of complete sets of vibrationally state-resolved cross sections and rate coefficients are reviewed, focusing on the relevant classes of collisional processes: resonant and non-resonant electron-impact excitation of molecules, atom–diatom and molecule–molecule collisions as well as gas-surface interaction. In particular, collisional processes involving atomic and molecular species, relevant to Earth (N_2, O_2, NO), Mars (CO_2, CO, N_2) and Jupiter (H_2, He) atmospheres are considered.

Keywords: elementary processes, excited states, non-equilibrium plasmas

(Some figures may appear in colour only in the online journal)

1. Introduction

Exploring new frontiers in the planetary system means facing problems connected to the engineering design of thermal protection systems to shield any space vehicle from searing re-entry conditions, which are characterized by intense heat flux to the craft nose and the sharp increase of temperature in the shock region. High-enthalpy hypersonic flow experiments, performed by scaling down the problem in wind tunnel facilities, are used for testing new materials for the tiles, the diagnostics and the characterization of the parameters of the plasma generated during the atmospheric impact. On the other

hand, the computational fluid-dynamic rebuilding of those experiments gives an insight into the physics governing the plasma temporal and spatial evolution and can be thought of as providing a virtual laboratory for the control of conditions in realistic configurations. These models assume thermal (if not chemical) equilibrium on the belief that non-equilibrium effects play a minor role in every realistic case of interest, and also in order to meet the requirement of computational efficiency. Attempts have been made to include non-equilibrium effects with multi-temperature approaches, integrating the detailed kinetics in different strategies, implementing macroscopic rate and multi-internal temperature models [1–4]. However under strong non-equilibrium conditions the temperature can neither characterize the internal distributions, whose overpopulated tails significantly affect the chemical kinetics, nor describe the structures in the electron energy distribution function (eedf), resulting in large deviations of the kinetic rates for electron-impact-induced processes from those obtained assuming a Maxwellian eedf. In this scenario, the state-to-state (StS) approach [5–8] can be considered the only reliable theoretical tool for the plasma modeling, self-consistently coupling the free-electron and chemical species collisional kinetics, and also including radiation models [9–12] accounting for radiative processes entering the energy global balance. In this context, we emphasize the role of radiation reabsorption by atoms and molecules in affecting the electron energy distribution function and, therefore, the macroscopic rates entering the kinetic approaches [12–14].

In StS models the chemical species in specific quantum states (electronically excited states, ro-vibrationally excited levels) are treated kinetically with independent master equations and characterized dynamically with state-specific cross sections and rate coefficients, with the reliability of the models and their predictive capability critically depending on the accuracy of the dynamical information [15–17]. Modern approaches in quantum molecular dynamics, combined with molecular beam experiments, have significantly enhanced and extended knowledge of elementary process probabilities and a number of web-accessible databases, which collect and validate data, are now available to the modeling community [18–20]. Data sets completeness, with respect to the vibrational ladder of the ground electronic state, allows the implementation of full vibrational kinetics for atmospheric diatomic molecules, also including metastable states, but still retains approximations for the treatment of rotational levels, considered in equilibrium with the translation degree of freedom.

In aerospace applications, dealing with dissociation and ionization regimes [21–28], a large number of elementary processes have to be included in the kinetic scheme, relevant to the main classes of electron impact, heavy particle collisions and heterogeneous processes. The collision dynamics is investigated by adopting different theoretical approaches, from quantum to semi-classical, quasi-classical and also simplified classical or phenomenological methods, that offer the most favorable balance between the level of approximation and the high computational load that usually characterize the calculation of complete sets, that avoid the scaling laws commonly used [29, 30].

The processes promoted by electron impact on the molecular target include vibrational and electronic excitations, dissociation and ionization, with progressively an increasing energy threshold. In the framework of an StS approach, the channels responsible for the vibrational pumping are of particular relevance, the most efficient of these being represented by the resonant vibrational excitation (RVE) mechanism:

$$e + \mathrm{M}_2(X, v_i) \rightarrow \mathrm{M}_2^- \rightarrow e + \mathrm{M}_2(X, v_f) \tag{1}$$

The resonant character of the process, with the temporary formation of the negative molecular ion, determines the features of the energy profile of the cross section, the threshold position, ensuring the effectiveness of collisions with low-energy electrons and, for many chemical systems, the significant enhancement in cross section with the increasing initial vibrational quantum number [31–34]. The negative ion can also evolve through alternative channels, leading to fragmentation, i.e. dissociative electron attachment and resonant dissociation [34, 35]. Dissociation can actually also occur through non-resonant direct excitation of electronically excited states, either purely repulsive or non-radiatively coupled to repulsive states through predissociation mechanisms

$$e + \mathrm{M}_2(X, v_i) \rightarrow e + \mathrm{M}_2^\star \rightarrow e + 2\mathrm{M} \tag{2}$$

usually characterized by high-energy thresholds. These channels and the dependence of the cross sections on the vibrational quantum number of the molecular target have been investigated with semi-classical approaches [36, 37], as in the case of direct ionization of H_2, O_2 and N_2 molecules [38–41]. The dissociation mechanisms have been widely investigated due to their efficiency in affecting the vibrational distribution, either by destroying the vibrational energy content or by forming atoms that are responsible for shaping the distribution tail through very effective vibrational deactivation in atom–molecule collisions (VT):

$$\mathrm{M}_2(X, v_i) + \mathrm{M} \rightarrow \mathrm{M}_2(X, v_f) + \mathrm{M} \tag{3}$$

The dynamics of heavy particle collisions on the relevant potential energy surface (PES) can be followed using the quasi-classical trajectory (QCT) method, which has proved to be accurate and compares well with quantum approaches. QCT provides robust trajectory statistics, and allows the characterization of single- and multi-quanta transitions through vibrational analysis in both reactant and product channels [42–51]. Rate coefficients are obtained with ro-vibrational resolution, but are usually included in kinetic codes as averages over the rotational distribution, which is assumed to be in equilibrium with the translation. Relying on the accuracy of the PES in the asymptotic regions, the QCT approach can also be used to estimate the probability of collisional induced dissociation:

$$\mathrm{M}_2(X, v_i) + \mathrm{M} \rightarrow 3\mathrm{M} \tag{4}$$

In molecule–molecule collisions the energy redistribution within the vibrational ladder operates through the $\mathrm{VT_M}$ and VV processes

$$\begin{aligned} &\mathrm{M}_2(X, v_i) + \mathrm{M}_2 \rightarrow \mathrm{M}_2(X, v_f) + \mathrm{M}_2 && (\mathrm{VT_M}) \\ &\mathrm{M}_2(X, v_i) + \mathrm{M}_2(X, w_i) \rightarrow \mathrm{M}_2(X, v_f) + \mathrm{M}_2(X, w_f) && (\mathrm{VV}) \end{aligned} \tag{5}$$

whose rates can be calculated in the framework of different theoretical approaches, including semi-classical [52–56] and quasi-classical trajectories [57], the forced-harmonic oscillator (FHO) [58–60] or the accurate close-coupled [61] methods. These approaches can also account for dissociation [59, 60, 62, 63].

Depending on the plasma conditions, a recombination regime can favor the energy pumping preferentially at the top of the vibrational ladder (three-body recombination):

$$\mathrm{M} + \mathrm{M} + \mathrm{M/M_2} \rightarrow \mathrm{M_2}(X, v_f) + \mathrm{M/M_2} \tag{6}$$

Recombination still represents a quite challenging process for direct dynamical investigation [64, 65]. However, in kinetic codes, usually the probability is derived, assuming microreversibility, through the principle of the detailed balance.

The interplay of these processes governs the plasma at a microscopic level in the gas phase. However, it should be stressed that in realistic simulation of plasma systems the interaction of the plasma with the reactor walls or, in simulation of entry conditions, the recombination at the thermal protection system (TPS) wall, must also be considered. This interaction significantly affects the vibrational kinetics, due to the formation of vibrationally excited molecules, through heterogeneous atomic recombination, or vibrational deactivation at the surface [66–70].

The three mechanisms commonly accepted for atom recombination at surfaces are:

- The Eley–Rideal (ER) mechanism in which a species impinging from the gas phase recombine with species previously adsorbed on the surface:

$$\begin{aligned} &\mathrm{A_{gas}} + \mathrm{wall} \rightarrow \mathrm{A_{ads}} * \mathrm{wall} \\ &\mathrm{A_{ads}} * \mathrm{wall} + \mathrm{B_{gas}} \rightarrow [\mathrm{AB}(v,j)]_{\mathrm{gas}} + \mathrm{wall} + \Delta E_{\mathrm{ER}} \end{aligned} \tag{7}$$

- The Langmuir–Hinshelwood (LH) mechanism in which two adsorbed species in close sites on the surface recombine:

$$\begin{aligned} &\mathrm{A_{gas}} + \mathrm{wall} \rightarrow \mathrm{A_{ads}} * \mathrm{wall} \\ &\mathrm{B_{gas}} + \mathrm{wall} \rightarrow \mathrm{B_{ads}} * \mathrm{wall} \\ &\mathrm{A_{ads}} * \mathrm{wall} + \mathrm{B_{ads}} * \mathrm{wall} \rightarrow [\mathrm{AB}(v,j)]_{\mathrm{gas}} + \mathrm{wall} + \Delta E_{\mathrm{LH}} \end{aligned} \tag{8}$$

- The hot-atom (HA) mechanism in which the impinging species becomes adsorbed but still possesses a high amount of energy. If this available energy is higher than the diffusion energy barriers, the adsorbed species could diffuse over the surface until they achieve adjacent sites that allow the final recombination of both adsorbed species [71].

The energy released in the recombination processes, ΔE, depends critically on the recombination mechanism, on the surface site where the species is pre-adsorbed and, therefore, on the nature of the atomic adsorption (whether chemi- or physisorbed). The energy released in the reaction can be shared among the degrees of freedom of the newly formed molecules (rotations, vibrations, translation and, possibly, electronic) and the degrees of freedom of the substrate (phonons and, possibly, electrons).

Different systems of interest in aerospace applications have been investigated using molecular dynamics (MD) studies by means of classical or quasi-classical trajectories [72–74] and semi-classical methods [75–82], by deriving the probability of recombination and the ro-vibrational nascent distributions.

The creation of a complete and consistent database of dynamical information for the StS modeling of re-entry non-equilibrium conditions, thus including all the processes discussed so far for the relevant planetary atmosphere chemical species, could be considered as one of the most challenging objectives of the fundamental research on elementary processes and as the essential prerequisite for any realistic attempt to use the StS models as a predictive tool.

This review offers a general overview of the information available to the modeling community, by focusing on molecular species relevant to Earth (N_2, O_2), Mars (CO_2, CO, N_2) and Jupiter (H_2, He) atmospheres. It discusses the theoretical results and attempts to assess their accuracy by comparison with experiments, although the measurements of probabilities, for processes involving excited states, are quite scarce due to the difficulty in preparing beams of molecules in selected quantum states. Hydrogen plasmas, relevant for Jovian atmosphere, will be discussed: for these plasmas vast knowledge and experience have been accumulated by different communities interested in problems such as divertors and negative ion source plasmas studied within thermonuclear fusion research [16, 83–87]. A specific section will be devoted to the CO_2 system, which is attracting a renewed interest due to the relevance of CO_2 plasmas in different technological applications for aerospace, energy and the environment [88–90]. The cross sections and rates for CO_2 processes will be reviewed [91–94] illustrating the complexity of constructing a vibrational kinetic model for a triatomic system [95].

2. Electron–molecule collisions

2.1. Non-resonant processes: vibronic excitation, dissociation and non-dissociative ionization

Reactive processes in electron–molecule collisions leading to dissociation and ionization can be regarded in the kinetic scheme as chemical source terms for atoms and electrons, significantly affecting the shape of the vibrational and electron distribution functions, respectively. These non-resonant channels have been investigated, in the past, with simplified theoretical approaches, classical [96], semi-classical [97–100] and phenomenological (BE*f*-scaling, *similarity approach*, and the binary-encounter-Bethe model) [39, 101–103], offering a computationally cheap route to derive a complete set and a reasonable accuracy for the dynamical information when compared with experiments and quantum scattering theories.

The dissociation of H_2, induced by electron collisions, can be regarded as a benchmark: in fact, the most efficient channel, represented by the dipole-forbidden excitation to

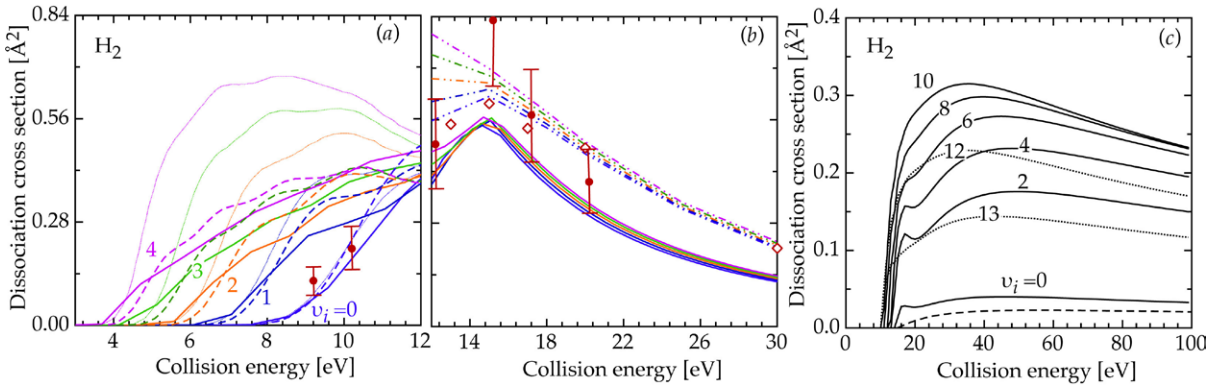

Figure 1. Dissociative excitation cross section of $b^3\Sigma_u^+$ state in e-H_2 collisions as a function of collision energy for different initial vibrational levels in (a) the threshold and (b) peak regions: solid lines [38], dashed–dotted lines [109], dotted lines [107], dashed lines [108]. Experimental results for $v_i = 0$: circles [105, 106], open diamonds [104]. (c) Direct dissociation cross section through singlets of H_2 as function of collision energy for different initial vibrational levels [38, 110], compared for $v_i = 0$ with [111].

the repulsive $b^3\Sigma_u^+$ state, has been well studied. Cross sections from the ground $v_i = 0$ level were estimated with accurate electron energy-loss spectroscopy (EELS) [104–106] and also the dependence on the initial vibrational level with different theoretical approaches, from the classical Gryzinski [38] to the quantum R-matrix [107, 108] and the complex Kohn variational approach [109], were investigated. Figures 1(a) and (b) display the energy profile, characterized by the near-threshold peak, also showing the expected shift in the threshold and a weak enhancement of the peak value for vibrationally excited molecules. General agreement is found among different approaches and for the $v_i = 0$ theoretical results mostly lie within the experimental uncertainties. Other channels contributing to global dissociation through predissociation mechanisms are, at relatively low-energies, the forbidden transitions to the first bound triplet states, $a^3\Sigma_g^+$ and the metastable $c^3\Pi_u$ [110]. It should be mentioned that the excitations involving triplets [112] are also of interest in kinetics, the Fulcher band ($a^3\Sigma_g^+ \rightarrow d^3\Pi_u$) being relevant to diagnostics of vibrational temperature in plasma. Increasing the electron energy, high-threshold excitations of dipole-allowed singlet terms ($B, B', B''\ ^1\Sigma_u^+$ and $C, D, D'\ ^1\Pi_u$) become accessible. These processes lead either to indirect vibrational pumping of the ground state through radiative decay (EV processes) [38], for excitations populating the discrete levels of the bound states, or to direct dissociation for transitions to the continuum of the electronically excited states. The theoretical direct dissociation cross sections, obtained using the semi-classical impact parameter method considering the contribution of all singlets [38, 110], are reported in figure 1(c) showing the large enhancement of the broad high-energy maximum with the increasing of the initial vibrational quantum number. The same figure compares the $v_i = 0$ cross sections with recent results obtained by normalizing to the optical oscillator strength [111] and predicting values a factor two lower. With the further increase in electron energy, ionization processes are activated in e-H_2 collisions. Dissociative and non-dissociative channels, proceeding through two different states of the molecular ion H_2^+ ($X^2\Sigma_g^+, ^2\Sigma_u^+$), have been studied within the classical approach [38, 110], deriving vibrationally resolved cross sections and showing the dominant role of the non-dissociative channel and the significant enhancement of ionization with the initial vibrational excitation of H_2. These results have been confirmed by recent calculations done in the same theoretical framework [113] and extended to consider ionizations initiated from electronically excited states.

Recently, direct dissociation cross sections for electron collisions with the He_2^+ molecular ion have also been computed [114]. The calculations were performed for the electronic transition $X^2\Sigma_u^+ \rightarrow A^2\Sigma_g^+$ starting from a given vibrational level of the ground state X and ending on the upper electronic state A whose potential curve is repulsive, so that dissociation occurs. The cross sections were calculated using the adiabatic nuclei approximation where the fixed-nuclei T matrices were obtained using the R-matrix method. The resulting cross sections show a low energy resonance peak, enhanced for vibrationally excited He_2^+ ions. For higher incident electron energies, a decreasing cross section trend is instead found increasing the vibrational excitation of the target.

Dissociation of $N_2(X^1\Sigma_g^+)$ and $O_2(X^3\Sigma_g^-)$ systems is mainly due to predissociation mechanisms following the excitations to bound excited states non-radiatively coupled with repulsive states. Cosby [115] gave experimental evidence of the large predissociation branching ratio in the vibronic excitation of singlet terms in the nitrogen energy diagram. Theoretical vibrationally resolved cross sections have been obtained, using the classical Gryzinski method, for a number of excitation transitions ($X^1\Sigma_g^+, \nu \rightarrow a^1\Pi_g, v' > 6; b^1\Pi_u; b'\ ^1\Sigma_u^+; c^1\Pi_u; c'\ ^1\Sigma_u^+; o^1\Pi_u; B^3\Pi_g$, $v' > 12; C^3\Pi_u, v' > 4$) involving both triplet and singlet states and, in a further step, combined with predissociation probability for the derivation of a global dissociative cross section [36, 116]. Figure 2(a) demonstrates the significant dependence of the cross section on the initial vibrational quantum number, as well as, for the $v_i = 0$ curve, the agreement with experimental dissociation measurements [115]. The O_2 dipole-allowed transition to the $B^3\Sigma_u^-$ state, origin of the well-known

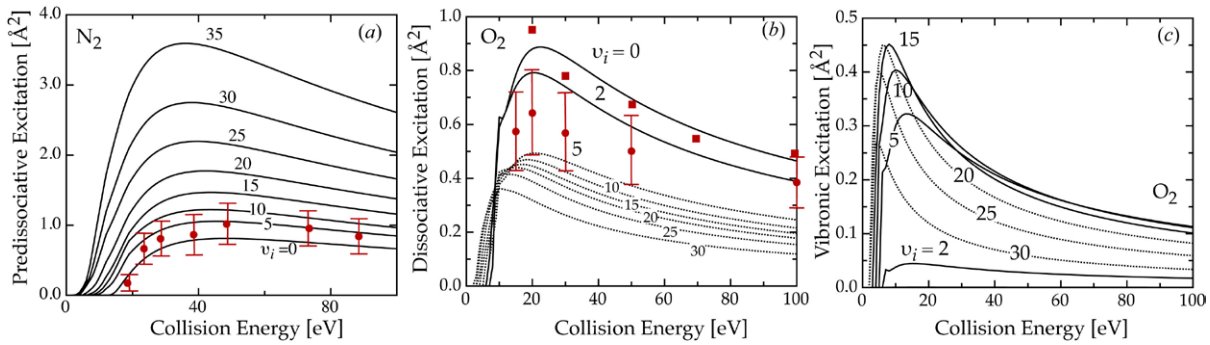

Figure 2. (a) State-specific global predissociation cross section in e-N_2 collisions as a function of collision energy for selected values of the initial vibrational quantum number [19, 36, 116], compared with experimental results for $v_i = 0$ (markers) [115]. Dissociative excitation (b) and vibronic excitation (predissociation) (c) cross section in e-O_2 collisions in the Schumann–Runge transition [37] as a function of energy for different initial vibrational levels, compared with experimental results for $v_i = 0$ [118] (circles) and electron-energy-loss experiments [117] (squares).

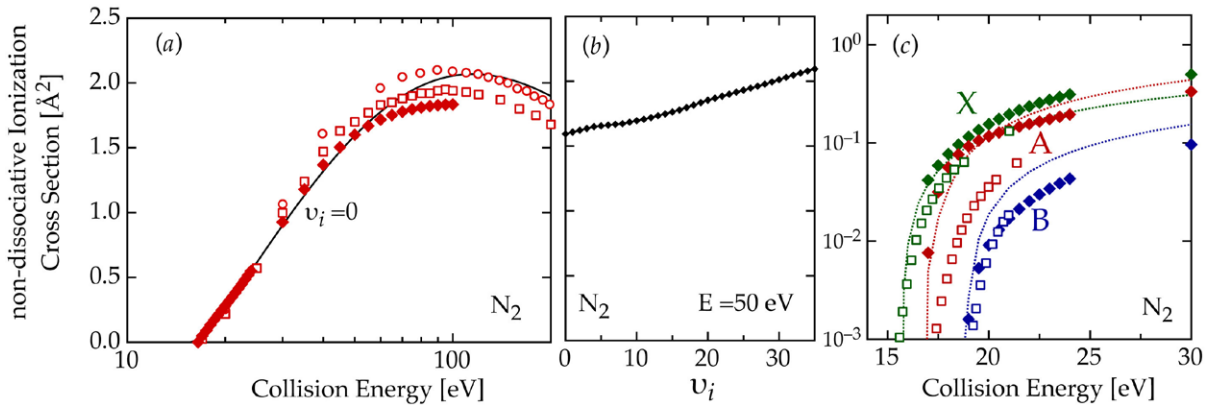

Figure 3. (a) Non-dissociative total ionization cross section of N_2 as a function of collision energy from the $v_i = 0$ vibrational level. (solid line) [40]; experimental results: (squares) [125], (circles) [126], (diamonds) [127]. (b) Vibrational profile of non-dissociative total ionization cross section at fixed collision energy. (c) Non-dissociative partial ionization cross sections as a function of collision energy from the $v_i = 0$ vibrational level. (dotted line) [40]; (close diamonds) [127]; (open squares) [128].

Schumann–Runge bands and continuum in the spectrum, provides two electron-impact-induced channels for dissociation through different mechanisms, i.e. the direct dissociation (figure 2(b)) and the predissociation of the vibrational level in the excited state (figure 2(c)), whose cross sections, obtained in the semi-classical approach [37], show opposite trends with the initial vibrational excitation of the target. The most important process from the $v_i = 0$ level is the dissociation to the continuum and, while older experiments [117] agreed quite well with theoretical results, recent EELS measurements [118] seem to predict slightly lower values for the integral cross section. It is worth noting that the excited states mainly responsible for predissociation, for both N_2 and O_2 systems, are also strongly affected by vibronic coupling effects, which leads to significant perturbations in the vibrational progression. The lowest three electronic terms of the $^1\Sigma_u^+$ and $^1\Pi_u$ spectroscopic series of N_2 exhibit a mixed valence–Rydberg character [119, 120], while the valence $O_2(B^3\Sigma_u^-)$ state is coupled with the $E^3\Sigma_u^-$ Rydberg state, leading to resonances known as *longest band* (LB), and *second band* (SB) transitions [121, 122]. A reformulation of the similarity approach has recently been proposed to include, in a simple way, non-adiabatic effects. This was validated for state-specific cross sections for N_2 [91], where the results were shown to be in very good agreement with recent EELS experiments [123, 124].

Cross sections for non-dissociative ionization, induced by high-energy electron collisions, have been obtained for nitrogen [39, 40] and oxygen [41], extending the classical theory for atoms to diatomic molecules [39]. Principal channels from the ground state have been included according to the following ionization schemes:

$$e + N_2(X^1\Sigma_g^+, \nu) \longrightarrow 2e + N_2^+(X^2\Sigma_g^+, A^2\Pi_u, B^2\Sigma_u^+) \quad (9)$$

$$e + O_2(X^3\Sigma_g^-, \nu) \longrightarrow 2e + O_2^+(X^2\Pi_g, a^4\Pi_u, A^2\Pi_u, b^4\Sigma_g^-) \quad (10)$$

Figure 3(a) compares the total ionization cross section for $N_2(v_i = 0)$ with experimental results [125, 126] and with values derived from experimental integrated electric dipole photoionization oscillator strengths [127]. Inspection of the vibrational profile for a selected value of the collision energy, in figure 3(b), shows clearly the weak dependence on the initial vibrational excitation of the molecule, this behavior being governed by the Franck–Condon superposition of the initial and final vibrational levels. The partial ionization cross sections of different channels, reported in figure 3(c),

Table 1. The first column shows the list of the reactions considered in the text occurring, according to the general scheme in (11), through the anionic resonant states shown in the second column. N_v is the number of vibrational levels belonging to the ground electronic state of the neutral molecule. The last column reports some relevant theoretical and experimental references.

REACTION	RESONANT STATES	N_v	Reference
$e + N_2(X\,^1\Sigma_g^+; v_i, j_i) \rightarrow e + N_2(X\,^1\Sigma_g^+; v_f, j_f)$	$N_2^-(^2\Pi_g)$	59	[32, 34, 132]
$e + N_2(X\,^1\Sigma_g^+; v_i, j_i) \rightarrow e + N(^4S) + N(^4S)$			[34]
$e + O_2(X\,^3\Sigma_g^-; v_i, j_i) \rightarrow e + O_2(X\,^3\Sigma_g^-; v_f, j_f)$	$O_2^-(^2\Pi_g,\ ^2\Pi_u,\ ^4\Sigma_u^-,\ ^2\Sigma_u^-)$	42	[31, 32, 133–135]
$e + O_2(X\,^3\Sigma_g^-; v_i, j_i) \rightarrow O(^3P) + O^-(^2P)$			[35, 136]
$e + O_2(X\,^3\Sigma_g^-; v_i, j_i) \rightarrow e + O(^3P) + O(^3P)$			[35, 136]
$e + NO(X\,^2\Pi; v_i, j_i) \rightarrow e + NO(X\,^2\Pi, v_f, j_f)$	$NO^-(^3\Sigma^-,\ ^1\Delta,\ ^1\Sigma^+)$	54	[32, 137, 138]
$e + NO(X\,^2\Pi; v_i, j_i) \rightarrow N(^4S) + O^-(^2P)$			[137, 139, 140]
$e + CO(X\,^1\Sigma^+; v_i, j_i) \rightarrow e + CO(X\,^1\Sigma^+; v_f, j_f)$	$CO^-(^2\Pi)$	81	[33]
$e + CO(X\,^1\Sigma^+; v_i, j_i) \rightarrow C(^3P) + O^-(^2P)$			[141, 142]
$e + CO(X\,^1\Sigma^+; v_i, j_i) \rightarrow C(^3P) + O(^3P)$			[141]
$e + H_2(X\,^1\Sigma_g^+; v_i, j_i) \rightarrow e + H_2(X\,^1\Sigma_g^+; v_f, j_f)$	$H_2^-(X^2\Sigma_u^+)$	15	[143–145]
$e + H_2(X\,^1\Sigma_g^+; v_i, j_i) \rightarrow H(^2S) + H^-(^1S)$			[143, 146–149]
$e + H_2(X\,^1\Sigma_g^+; v_i, j_i) \rightarrow H(^2S) + H(^2S) + e$			[150]
$e + H_2(X\,^1\Sigma_g^+; v_i, j_i) \rightarrow e + H_2(X\,^1\Sigma_g^+; v_f, j_f)$	$H_2^-(B^2\Sigma_g^+)$	15	[143]
$e + H_2(X\,^1\Sigma_g^+; v_i, j_i) \rightarrow H(^2S) + H^-(^1S)$			[143]
$e + H_2(X\,^1\Sigma_g^+; v_i, j_i) \rightarrow H(^2S) + H(^2S) + e$			[150]
$e + H_2(X\,^1\Sigma_g^+; v_i, j_i) \rightarrow e + H_2(X\,^1\Sigma_g^+; v_f, j_f)$	$H_2^-(^2\Sigma_g^+$, Rydberg state)	15	[83, 87, 91]
$e + H_2(X\,^1\Sigma_g^+; v_i, j_i) \rightarrow H(^2S) + H^-(^1S)$			[84, 86, 91, 151, 152]

demonstrate the agreement of classical estimation with the old Gryzinski method [128] and recent results [127], also confirmed by the values of branching ratios, $\eta^{\text{theo}}_{X^2\Sigma_g^+} = 0.301$, $\eta^{\text{theo}}_{A^2\Pi_u} = 0.494$, $\eta^{\text{theo}}_{B^2\Sigma_u^+} = 0.204$ [39, 40], well comparing with inferred estimates at 100 eV by Van Zyl & Pendleton [129] ($\eta^{\text{exp}}_{X^2\Sigma_g^+} = 0.320 \pm 0.147$, $\eta^{\text{exp}}_{A^2\Pi_u} = 0.535 \pm 0.112$, $\eta^{\text{exp}}_{B^2\Sigma_u^+} = 0.145 \pm 0.017$). For the O_2 system [41] the classical theory of ionization was able to predict the dominant role of the $O_2^+(X^2\Pi_g)$ experimentally observed, and also the absolute value of partial cross sections at 100 eV, $\sigma^{\text{theo}}_{X^2\Pi_g} = 0.874$ Å^2, $\sigma^{\text{theo}}_{a^4\Pi_u} = 0.474$ Å^2, $\sigma^{\text{theo}}_{b^4\Sigma_g^-} = 0.183$ Å^2, well reproducing the direct experimental estimates of [130], $\sigma^{\text{exp}}_{X^2\Pi_g} = 0.922 \pm 0.184$ Å^2, $\sigma^{\text{exp}}_{a^4\Pi_u} = 0.508 \pm 0.102$ Å^2, $\sigma^{\text{exp}}_{b^4\Sigma_g^-} = 0.221 \pm 0.044$ Å^2. However large discrepancies exist between branching ratios determined by the role of the $A^2\Pi_u$ channel, experimentally found to be negligible.

2.2. Resonant processes: vibrational excitation, dissociation and dissociative attachment

Electron–molecule resonant collisions play an important role in the chemistry of atmospheric plasmas as they provide efficient channels for internal excitation or dissociation of molecules. The collision mechanisms, according to the well-known resonance model, are based on the temporary trapping of the projectile electrons by the target such that the molecular anion thus formed (also called the resonant state) has a finite lifetime, during which the electron can auto-detach, leaving behind either an excited molecule or a fully dissociated molecule when this is excited to a vibrational continuum. Electronic excitations can also occur through a resonant collision, but transitions among the ro-vibrational levels of the ground electronic states are of particular interest due to their fundamental role in the atmospheric gas kinetics. On the other hand, if the lifetime of the resonant state is sufficiently long, it can lead to dissociative electron attachment (DEA) forming a neutral atom and an atomic anion. If M_2 represents a diatomic molecule, and v_i, j_i and v_f, j_f two ro-vibrational energy levels of the same electronic state then one has, schematically:

$$e + M_2(v_i, j_i) \rightarrow M_2^- \rightarrow \begin{cases} M_2(v_f, j_f) + e & \text{ro-vibrational excitation} \\ M + M + e & \text{dissociation} \\ M + M^- & \text{dissociative attachment} \end{cases} \tag{11}$$

where M_2^- is the molecular negative ion in a resonant electronic state, M is a neutral atom and M^- is a negative atomic ion. Cross sections for these resonant processes have been calculated and measured for many molecules relevant to atmospheric plasmas. Table 1 shows the resonant processes for the main species for which cross section data are presently available. All the diatomic

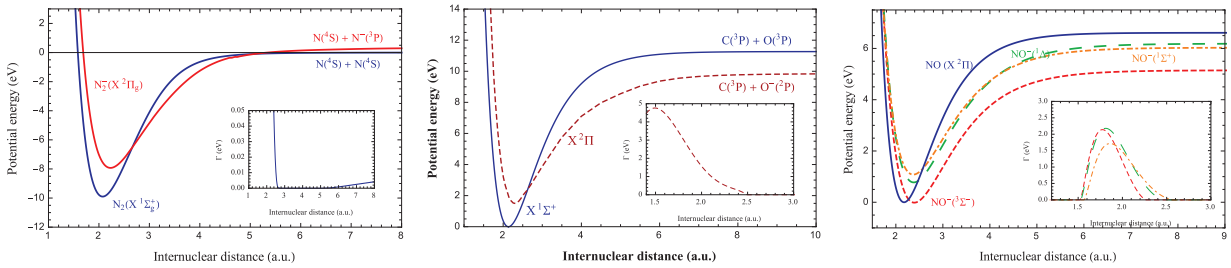

Figure 4. Potential energy curves for neutral and resonant states of N_2, CO and NO molecules. The small box in each panel shows the corresponding widths [32–34].

molecules included in the table are initially in their ground electronic state. The second column shows the electronic term symmetry of the resonant states M_2^- involved in the process. For hydrogen molecules, cross sections are available for resonant processes occurring through three resonant states, two of which, $X^2\Sigma_u^+$ and $B^2\Sigma_g^+$, arising from H_2 valence states ($X^1\Sigma_g^+$ and $b^3\Sigma_u^+$) and a third Rydberg-excited state, of $^2\Sigma_g^+$ symmetry, generated from several excited states of the target molecule [131]. From a theoretical point of view, the first step for the cross section calculation is the computation, for a suitable range of internuclear distance R, of the potential energy curves, $V(R)$ and $V^-(R)$, for the electronic states of both the stable and resonant molecular species M_2 and M_2^- respectively, as well as the computation of the resonance width, $\Gamma(R)$, of the M_2^- unstable state, linked to its lifetime, τ, by $\tau(R) = \hbar/\Gamma(R)$. While the potential curve for the target state, $V(R)$, can be obtained by means of standard electronic structure calculations, the adiabatic resonance potential $V^-(R)$ (resonance energy positions) and the width $\Gamma(R)$ must be calculated by solving the fixed-nuclei electron–molecule collision problem. Among the many methods developed over the years for treating the scattering event [153–156], recently the R-matrix method has been widely used, for the collision systems of table 1, to provide the above curves and widths necessary for nuclear motion studies of the resonant processes (see section 2.4). A brief account of this method is given in the next section.

2.3. R-matrix methods

The R-matrix method is a rather general scattering formalism [157] which has been heavily adapted for treating electron–molecule collision calculations [155]. The physical basis of the R-matrix method is the division of the electron collision space into two regions: an inner region in which the complicated electron interaction with the target is treated in full and an outer region where the electron is assumed to move simply in the long-range potential due to the target. This representation of the problem has considerable algorithmic [158] and computational advantages which are discussed in detail in the references cited above. In particular, it is only for the outer region that the calculation needs to be repeated as a function of collision energy which means that performing calculations for many energies is computationally efficient.

As we have seen in the previous section, one feature of electron collisions with molecules is the temporary trapping of electrons in quasi-bound states which give rise to resonances. Within the Born–Oppenheimer approximation, for each resonance energy position, a width can be extracted from the scattering calculations by a number of methods such as fitting the eigenphases of the collision [159] or analyzing the time-delay of the collision process [160]. For broad (short-lived) resonances it can be necessary to account for effects beyond the Born–Oppenheimer approximation by considering the energy dependence of the resonance; such calculations, based in the so-called *non-local model* [161, 162], briefly discussed in the next section, are possible within the $R-$matrix method [163], but have not been found necessary for the studies reviewed here.

Figure 4 shows some examples of potential curves for the ground states and the resonant states (see table 1) of CO, N_2 and H_2 molecules, as well as the corresponding widths, obtained by the R-matrix method.

The ability to study electron scattering at a fine grid of energies means that resonance parameters can be mapped out in detail [164]. It is possible to look at highly excited bound states in similar detail by performing scattering calculations at *negative collision energies* [165], however, the approach adopted for some of the system in table 1 has largely been to use standard bound state molecular electronic structure codes such as MOLPRO [166] for such purposes.

2.4. The role of nuclear dynamics in resonant processes

When an electron is trapped by a neutral N-electron molecule a resonant negative molecular ion is formed in a given electronic state and the nuclei motion takes place in the potential field, $V^-(R)$, of N + 1 electrons. Quasi-bound ro-vibrational levels then arise which may decay through the channels represented in equation (11). From a theoretical point of view, if the resonant state is sufficiently stable, the Born–Oppenheimer separation of electrons and nuclei motions can be applied. This is the physical basis of the so-called *local complex potential model*, a theoretical description of the nuclei dynamics which provides the cross section expressions for the nuclear processes in (11). This model gives quite satisfactory results in many cases, and cross sections for many of the reactions listed in table 1 have been obtained using this model. However, as already noted in the previous section, in cases of particular unstable resonant states, as for example that arising in electron-H_2 scattering, where the electron is trapped by the molecule via a centrifugal barrier and rapidly tunnels away, a more complete treatment of the electron–molecule collision, which goes to some extend beyond the Born–Oppenheimer

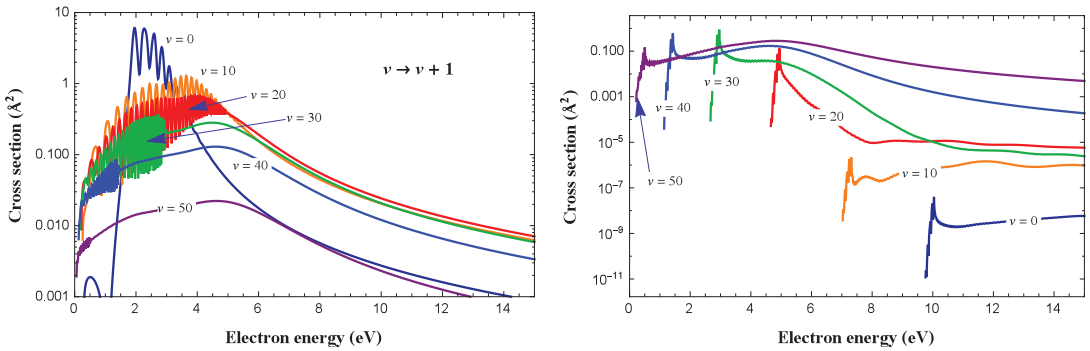

Figure 5. Electron-N_2 cross sections for one-quantum vibrational excitation and resonant dissociation [34].

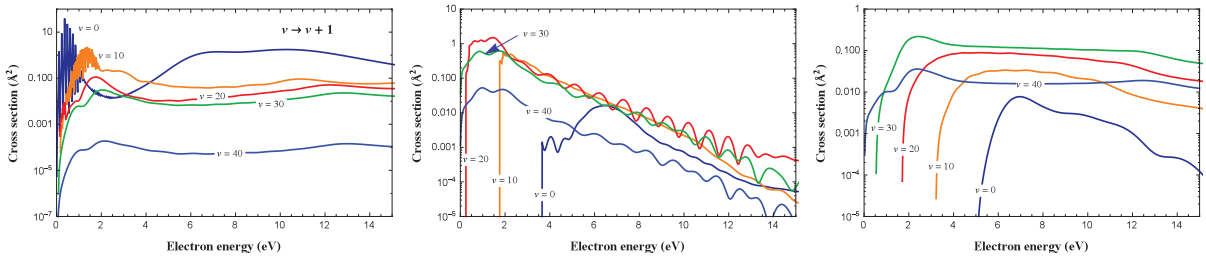

Figure 6. Electron-O_2 cross sections for one-quantum vibrational excitation, DEA and resonant dissociation [31, 35].

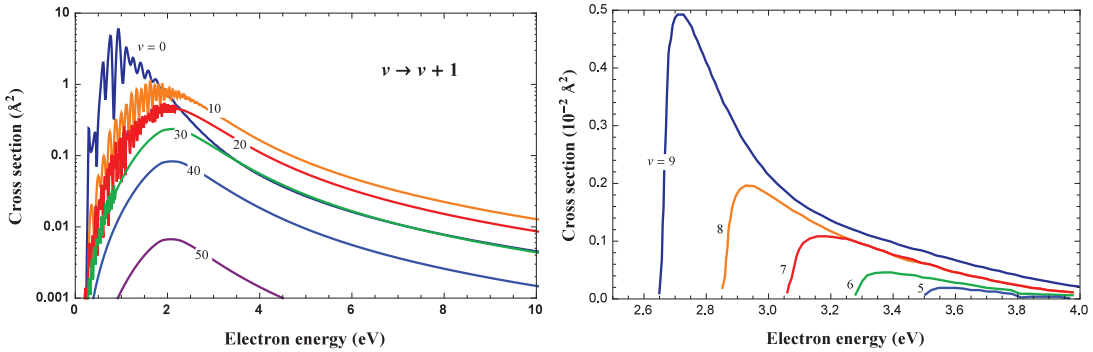

Figure 7. Left panel: electron-NO scattering cross sections for one-quantum vibrational excitation [32] (left panel) and dissociative attachment for some initial vibrational level [137] (right panel).

approximation, is required such as that provided by the non-local model [156]).

2.5. Resonant cross sections

Figure 5 (left panel) shows calculated local cross sections for resonant vibrational excitation in N_2, as a function of energy and for some initial vibrational level v_i, for one-quantum transitions ($\Delta v_i = 1$). These transitions are usually characterized by quite large cross sections which means they play an important role in vibrational kinetics. The oscillatory structures in the cross sections are attributable to the quasi-bound vibrational wave functions of the resonant state. Figure 5 (right panel) displays the cross sections for resonant dissociation which show significant values for very high vibrational levels only [34]. These two processes occur, according to the mechanisms in equation (11), through the resonant state of symmetry $^2\Pi_g$, generated by the formation of a centrifugal barrier (shape resonance). Dissociative attachment, instead, from this resonant state is not an allowed process as the atomic ion, N^-, produced in the dissociation is unstable, owing to a positive electronic affinity [167–169]. Cross sections for the same resonant processes for the O_2 molecule, including dissociative attachment, are shown in figure 6. In this system, four resonant states (see table 1), formed by adding the extra electron to one of the HOMO–LUMO molecular orbitals of the ground state configuration of the target molecule, contribute to the collision [31, 35]. Figure 7, finally, shows the cross sections for resonant one-quantum vibrational excitation [32] of nitric oxide molecules and dissociative attachment for some selected initial vibrational levels, the latter calculated using the non-local model [137]. Also, for this reaction three resonant states take part in the collision.

For the CO molecule cross sections for vibrational excitation by electron impact, occurring through the resonant electronic state $^2\Pi$ of table 1, were calculated using the *R*-matrix potentials and widths shown in figure 4 [33]. Recently, cross-section calculations were extended to the DEA and resonant dissociation processes, involving the above resonant state, as

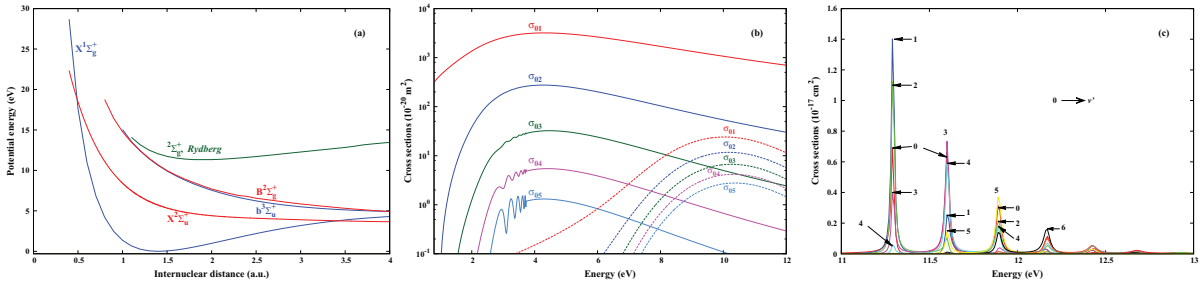

Figure 8. Panel (a): potential energy curves for the H_2^- resonant states along with the $X^1\Sigma_g^+$ and $b^3\Sigma_u^+$ target states. Panel (b): cross section for the H_2 vibrational excitation occurring through the $X^2\Sigma_u^+$ and $B^2\Sigma_g^+$ resonances [143]. Panel (c): same process as in (b) but occurring through $^2\Sigma_g^+$ Rydberg resonances [87].

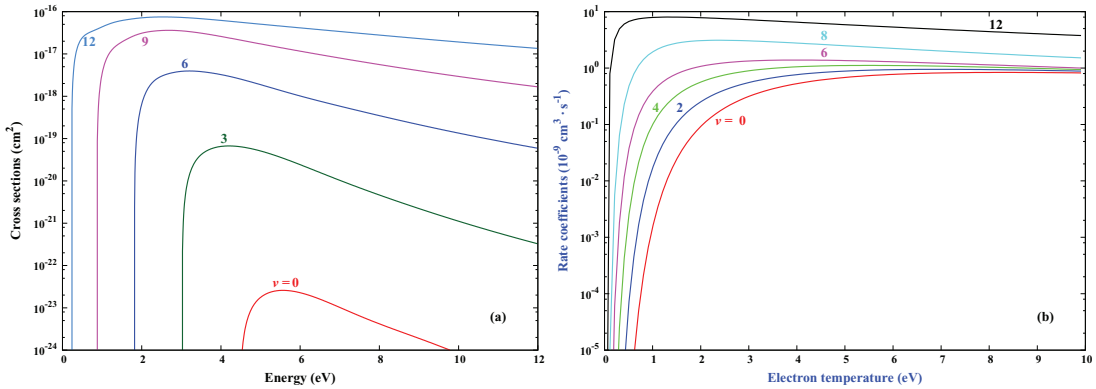

Figure 9. (a) Cross section for the resonant dissociation process, occurring through the $X^2\Sigma_u^+$ resonant state, [150] and (b) the corresponding rate coefficients as a function of the electron energy and temperature respectively.

a function of the vibrational excitation of the molecule. The results are reported in [141].

Once the cross sections are known, rate coefficients for the resonant processes can be obtained if one assumes that in the plasma system electrons are found in thermal equilibrium. In this case, the analytic Maxwellian energy distribution function can be used to average the collision cross sections. Calculated rate coefficients, which are of fundamental importance in kinetic modeling of plasmas, are now available for most of the reactions in table 1 and can be found in the literature quoted in the same table.

The hydrogen molecule occupies a prominent place in the studies of resonant processes, both for the strong interest that it draws in many applicative areas and for its simplicity, which makes it suitable for investigations of the collision mechanisms and for testing theories. In the next section some historical results and recent developments are reviewed.

2.6. *Resonant collisions involving* H_2 *molecule*

In the range of energy from few eV to approximately 15 eV, three distinct resonant states of H_2^- (see figure 8(a) contribute significantly, each with its own characteristic peak behavior for various resonant processes. For electron energy between 2 eV and about 8 eV, the $X^2\Sigma_u^+$ resonant state of H_2^- dominates all resonant processes. For energies between 8 eV and about 12 eV, the lowest excited $B^2\Sigma_g^+$ state of H_2^- controls various resonant processes. For electron energies in the range from 11 eV to about 15 eV, the resonant processes are regulated by the $^2\Sigma_g^+$ excited Rydberg electronic state of H_2^-.

The resonant vibrational excitation (RVE) cross sections σ_{v_i,v_f} of H_2, for the process occurring through the lowest two resonant states, are shown in figure 8(b). In this figure, all the cross sections start from $v_i = 0$. Interestingly, near 10 eV, the RVE cross sections σ_{01} and σ_{02} are dominated by the $X^2\Sigma_u^+$ state while the excitation of higher levels occurs predominantly through the $B^2\Sigma_g^+$ state. The RVE cross sections, shown in figure 8(c) for $v_i = 0$, are determined by the excited $^2\Sigma_g^+$ Rydberg state of the molecular ion H_2^-. For each value of v_f these cross sections show multiple peaks with the dominant peak shifting progressively to a higher energy as v_f is increased.

The two lowest resonant states of H_2^-, $X^2\Sigma_u^+$ and $B^2\Sigma_g^+$, contribute significantly to the dissociation of H_2. Because of the positioning of their potential energy curves, the $X^2\Sigma_u^+$ resonance decays only to the continuum of the H_2 ground electronic state $X^1\Sigma_g^+$. The $B^2\Sigma_g^+$ resonance, on the other hand, can decay to both the continua of $X^1\Sigma_g^+$ and $b^3\Sigma_u^+$ states of neutral H_2. Figure 9(a) illustrates the contribution of the $X^2\Sigma_u^+$ resonance to the cross sections for dissociation of H_2 for several different v_i and shows the strong cross section dependence on the initial vibrational level of the molecule. The peak value, in fact, increases by almost seven orders of magnitude as v_i increases, as already observed for N_2 (see figure 5(b)). On the other hand, the contribution of the $B^2\Sigma_g^+$ resonance to the

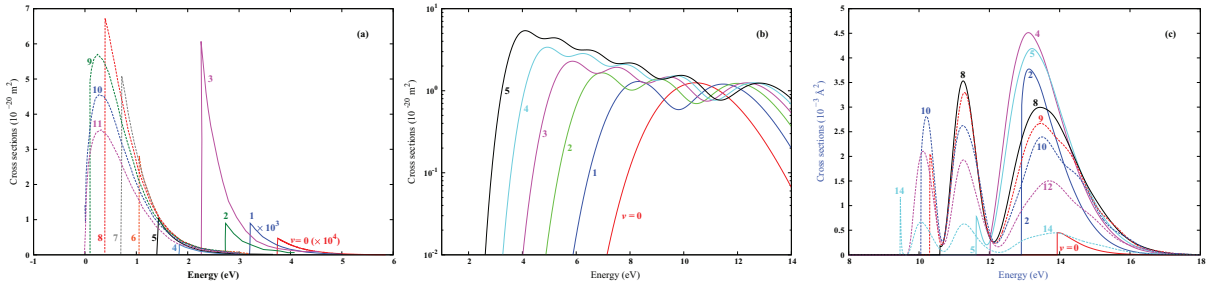

Figure 10. Dissociative electron attachment cross section occurring through the (a) $X^2\Sigma_u^+$ [144], (b) $B^2\Sigma_g^+$ [170] and (c) $^2\Sigma_g^+$ Rydberg state [151], as a function of the incident electron energy and for different v_i.

dissociation cross sections (not shown) as a function of energy presents oscillatory behavior [150] and, for small values of v_i, its contribution to the dissociation cross sections becomes larger than that of the $X^2\Sigma_u^+$ resonance. No data are currently available for dissociation occurring through the Rydberg state. Figure 9(b) shows the *total* Maxwellian rate coefficients, i.e. the sum of all the above contributions to the H_2 dissociation, as a function of average electron energy and for different levels v_i. For each level, the dissociation rate exhibits a broad maximum which increases rapidly as v_i is increased.

The shape of the DEA cross section depends on the nature of the H_2^- resonant state. For example, in the energy range below 5 eV, the $X^2\Sigma_u^+$ resonant state contributes significantly to the DEA cross section. Furthermore, this cross section depends very sensitively on the initial vibrational energy of the neutral H_2 molecule. This sensitivity can be appreciated in figure 10(a) which shows DEA cross sections as a function of electron energy for various values of v_i calculated using the non-local model approach [144, 149]. Figure 10(b) shows the cross sections for dissociative electron attachment to H_2 proceeding through the formation of $B^2\Sigma_g^+$ resonance. In this case, there is no significant enhancement of the DEA cross-section, even if H_2 molecule is initially vibrationally excited. Figure 10(c) shows DEA cross sections as a function of electron energy, proceeding via the $^2\Sigma_g^+$ Rydberg resonance, for different values of v_i. This state dissociates into H^- and an $n = 2$ excited hydrogen atom. Interestingly, in this case there is not much enhancement of the cross section with increasing v_i. However, since the threshold for the DEA cross section is lowered as the vibrational level is increased, additional peaks of the cross section are revealed.

2.7. Further resonant processes

The electron–molecule reactions sketched in equation (11) do not exhaust all the possible resonant collisions. Associative detachment, for example, is also a resonant process which leads to molecular neutral species [171, 172]. It can be considered the inverse of dissociative attachment and its cross sections can be linked to the DEA ones by the principle of detailed balance.

Dissociative recombination is yet another process of great importance in plasma kinetics. This process involves a positive molecular ion, M_2^+, which after capturing the incident electron, can give rise to a neutral molecule in an unstable state toward electron re-emission. However, if the molecule is found in a repulsive state, typically a super-excited electronic state, $M_2^{\star\star}$, or in a bound Rydberg state, $M_2^{\star}$, which can predissociate, breakdown of the molecular bond occurs. These two mechanisms are usually denoted as direct and indirect dissociation. Dissociative recombination cross section data have been produced for many molecules of atmospheric interest [173–175]. Among the vast literature a wide and up-to-date overview of the dissociative recombination process can be found in [176].

3. Heavy particle collisions

3.1. Collision dynamics simulations

The calculation of molecular collisions observables, such as energy transfer cross sections and rate coefficients for gas phase systems is highly demanding already for masses, energies, temperatures and complexity of the interaction typical of the moderately large systems involved in the simulations. When more than three atoms are involved in a collision, it is impractical (and so far has not been attempted) to ground realistic simulations and related systematic computations on full dimensional quantum treatments integrating the associated scattering Schrödinger equations [177]. Because of this, related computations are usually carried out running QCT programs [178] or sometimes by combining quantum mechanics treatments (for selected bound degrees of freedom) with classical mechanics ones (for the remainder) within the so-called quantum-classical method [179]. Rarely, and almost exclusively for three atom systems, the calculation is performed using exact quantum full-dimensional treatments [180].

Recently, a computation scheme has been implemented, using a distributed workflow in a grid empowered molecular simulator (GEMS) [181], that considers, in a sequence, the *ab initio* calculation of the electronic structure of the molecular system, its functional representation as an analytic PES spanning the whole configuration space covered by considered process, the detailed evaluation of the StS dynamics of the system, and the statistical combination of the resulting detailed quantities to assemble *ab initio* generated observables. Once the PES has been built and validated against accurate spectroscopic and scattering information (including possible iterations), calculations are run to get reliable estimates of

the cross section and rate coefficient values to feed as input to realistic simulations under different conditions (including those for which experiments cannot be performed). To ensure statistical accuracy large batches of classical trajectories are run and from their outcomes StS transition probabilities as well as detailed cross sections and rate coefficients for large numbers of ro-vibrational states, over a wide range of energies and temperatures, are obtained [42–44]. In this respect, the use of QCT techniques on parallel and distributed computing infrastructures has been the winning move of recent times because of the perfect decoupling of individual trajectories (or of small batches of them). However, the reliability of the results depends on the suitability of the QCT method for describing the collision process and on the accuracy of the PES in modeling long- and short-range intermolecular forces.

3.2. Molecule–molecule collisions

3.2.1. Potential energy surfaces for the energy transfer. Even if, in principle, the intermolecular potentials can be characterized in detail by molecular beam scattering experiments [182] and spectroscopic studies of van der Waals complexes [183], the inference from the measured data is a difficult inversion problem. An accurate PES can be obtained by an efficient GEMS procedure that adopts a parametric model potential and then tentatively varies the value of the parameters so as to obtain from the integration of the dynamical equations the best possible agreement with experimental results to reproduce the glory oscillations and the second virial coefficient for diatom–diatom systems [55]. Moreover, since vibrations and rotations distort the molecular geometry, affecting both polarizability and charge distribution, the intermolecular forces related to such properties are strongly dependent on the quantum states of the interacting monomers and so are the outcomes of collision events. A suitable intermolecular potential energy surface should, therefore, definitely return the variations of the interaction with the internal coordinates of the molecules. For this reason, those dimer PESs made of frozen monomer interaction terms cannot be considered truly adequate for modeling the energy transfer in gas phase systems and full-dimensional PESs should be provided instead.

For these reasons V, the functional representation of the PES of the two colliding molecules, should contain both the intermolecular component V_{inter} (representing the interaction of the two molecules depending, as shown below in equation (12), on the center-of-mass distance R between the two molecules and on the angles Ω denoting the set of angles defining their mutual orientation) and the intramolecular one V_{intra} (representing the potential energy function of the two isolated molecules at infinite separation depending on the vector $\mathbf{q}$ defining the internal coordinates of the two molecules). Accordingly, V is formulated as a sum of these two contributions:

$$V = V_{\text{intra}}(\mathbf{q}) + V_{\text{inter}}(R, \Omega; \mathbf{q}). \tag{12}$$

Note that V_{inter} depends parametrically on the molecular geometry $\mathbf{q}$ in order to incorporate the effects of the ro-vibrational motion on the intermolecular forces. The internal interaction energy V_{intra} is often replaced by an *ab initio* ground state potential, while V_{inter}, the interaction component pivoting the energy transfer, has to be accurately determined in order to ensure the realism of the simulations and the accuracy of the energy transfer probabilities, cross sections and rates.

A general versatile formulation of the term V_{inter} of equation (12) consists of a sum of two effective interaction components, i.e. V_{vdW} and V_{elect}, representing the van der Waals (size repulsion plus dispersion attraction) and the electrostatic reactant interactions, respectively. These two terms vary strongly with R while weakly depending on Ω. V_{elect} depends on the anisotropy of the charge distributions of the two molecules and tends to the permanent-quadrupole–permanent-quadrupole interaction at large distances. However, when the two molecules come into closer contact during the collision (as is the case of long-lasting collisions) the interaction between atoms originally belonging to different molecules should be taken into account more explicitly. This is usually done by formulating the van der Waals term as an improved Lennard-Jones (ILJ) potential [184], adding further flexibility to the PES.

A more general approach, is to combine contributions from different arrangements of the system already in the fitting procedure. A great advantage of these so-called *local* methods is the fact that the fitting can be improved by simply adding more *ab initio* points from nearby. Moreover, the points need not be located on a uniform grid. This is the case of the moving least squares (MLS) techniques which mix together global and local (basis functions which are only used locally to the geometry of interest) features of the interaction [185–189]. The enforcement of the symmetry of the system on the formulation of the PES can also be adopted. In preliminary studies of the $N_2 + N_2$ [55] and $O_2 + N_2$ [190] energy transfer processes, reference is made to ILJ basis functions.

3.2.2. Quasi-classical and quantum-classical calculations. A multi-dimensional PES of the type of equation (12) for a four-atom colliding system can be used to run QCT simulation at a StS level of details, accounting for the quantization of reactants and products.

The initial vibrational states of the colliding molecules are explicitly selected [92, 184, 191–193], while the initial rotational states are assigned by sampling a Boltzmann distribution at a given rotational temperature T_{rot}. This means that cross sections and probabilities obtained from the trajectories are specific for vibrational states, but thermally averaged over rotations. Note that rotational averaging reduces the number of quantum labels that have to be taken into account and also the computational load. For the selection of the initial velocity of trajectory two main alternatives exist: (i) velocities are selected to give a fixed collision energy E; (ii) velocities are selected randomly from a Boltzmann distribution at temperature T (translational temperature). The second option directly gives a set of initial and final states whose processing results in thermal probabilities and rate coefficients, assuming translation and rotational degrees of freedom in equilibrium ($T_{\text{rot}} = T$). The set of final product states have to be presented in a quantum fashion by a quantization procedure. The simplest representation of the vibrational energy of diatomic

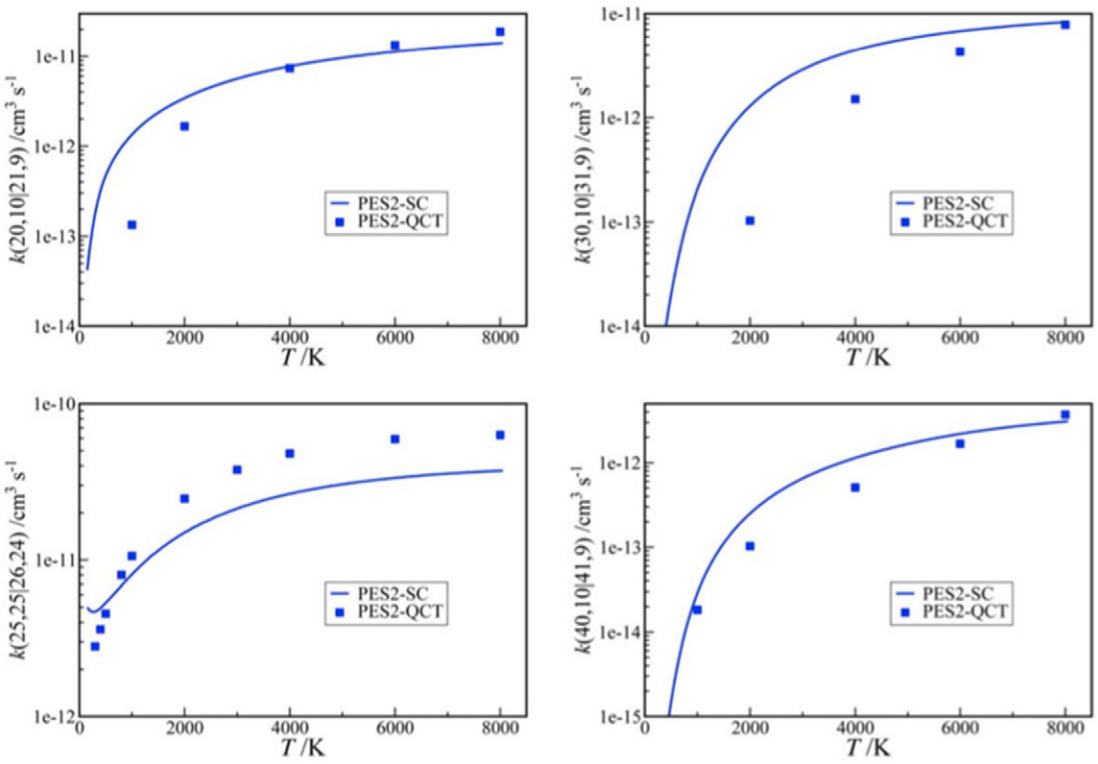

Figure 11. QCT (markers) and semi-classical (solid lines) rate coefficients [55] as a function of temperature for the transitions: $N_2(v_a) + N_2(v_b) \rightarrow N_2(v_a + 1) + N_2(v_b - 1)$). Upper-left panel: ($v_a = 20, v_b = 10$); upper-right panel: ($v_a = 30, v_b = 10$); lower-left panel: quasi-resonant ($v_a = 25, v_b = 25$); lower-right panel: ($v_a = 40, v_b = 10$).

and triatomic molecules is obtained by approximating the vibrational motion as that of a set of independent harmonic oscillators. In this way the energies of each vibrational mode can be obtained by projecting the final phase-space vectors of the products into the normal-mode vectors. Accordingly, a data-binning can be performed to obtain vibrational quantum numbers by simply rounding the ratios of the energy content of each vibration mode to the corresponding energy spacing to the closest integer. A slightly more accurate procedure relies on the Einstein–Brillouin–Kramer (EBK) quantization rule, based on the action integral, for each vibrational coordinate (e.g. a normal mode), over an entire period. After the action integrals, the obtained 'non-integral' quantum numbers have to be binned.

As already anticipated, a more rigorous approach (and therefore a more significant validation test of the results obtained) has been taken for the $N_2 + N_2$ [55] and $O_2 + N_2$ [190] systems by employing quantum-classical treatments. The goal of such an effort has been, on the one hand, to calculate an accurate sets of vibrationally selected rate constants for multi-quantum VV and VT exchanges in a broad range of gas temperature and, on the other hand, to evaluate the conditions in which the QCT treatment agrees better with quantum-like treatments. For the diatom–diatom systems considered, one can treat molecular vibrations quantum-mechanically by integrating the related time-dependent Schrödinger equations while treating rotation and translation classically by integrating the related Hamilton equations. The two subsystems, and the corresponding equations of motion, are dynamically coupled through

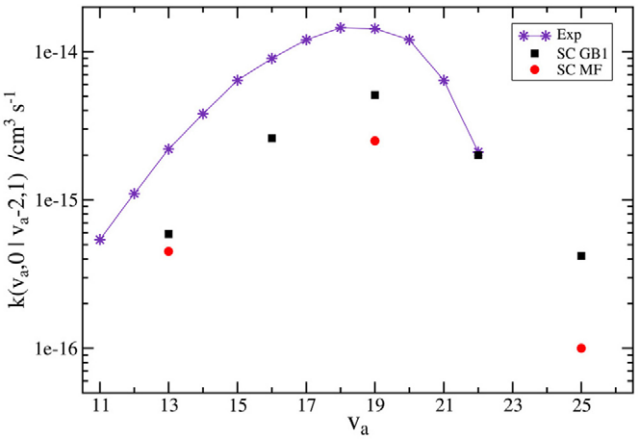

Figure 12. The $O_2(v_a) + N_2(v_b = 0) \rightarrow O_2(v_a - 2) + N_2(v_b = 1)$ semi-classical rate coefficients at $T = 300$ K calculated and compared with experimental results of [197].

the definition and calculation of a time-dependent 'effective' Hamiltonian and the time evolution of the total wave function is obtained by expanding it over the manifold of the product of, rotationally distorted Morse wave functions of the two isolated molecules. Then, the Hamilton equations for the ro-translational motions are integrated self-consistently together with the Schrödinger equations of motion of the vibrational amplitudes (the number of vibrational levels, above and below the initial vibrational state of the colliding diatoms included in the wave function expansion, depends on the initial vibrational state of both molecules and on the impact

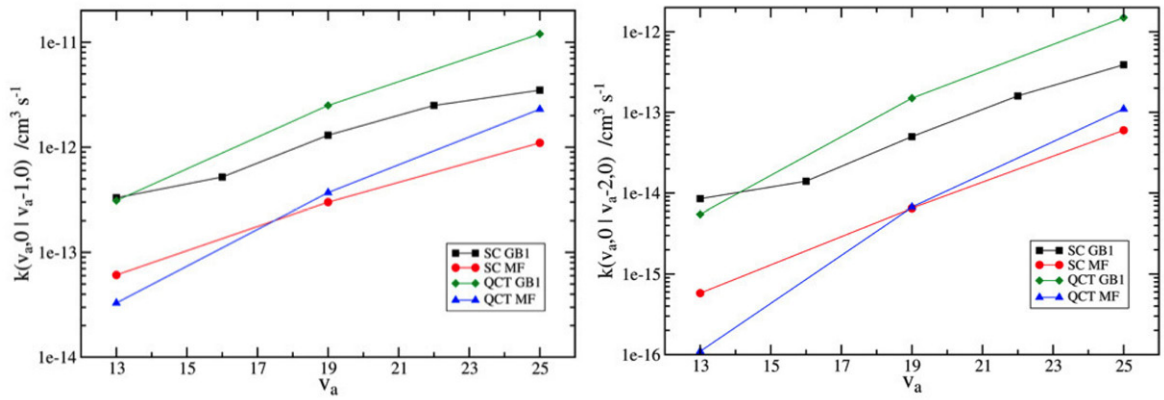

Figure 13. SC and QCT rate coefficients at $T = 1000$ K calculated on GB1 [198] and MF [190] for single (left panel) and double (right panel) quantum vibrational de-excitation of the process $O_2(v_a) + N_2(v_b = 0) \rightarrow O_2(v_a') + N_2(v_b' = 0)$.

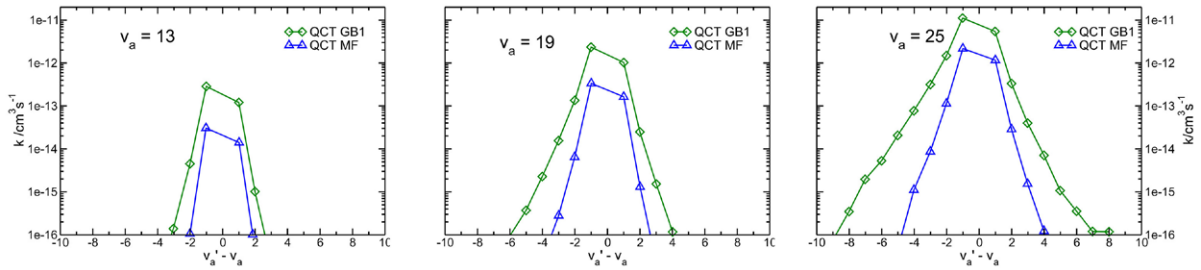

Figure 14. QCT rate coefficients at $T = 1000$ K calculated on GB1 [198] and MF [190] PESs for multi-quantum vibrational excitation and de-excitation of the process $O_2(v_a) + N_2(v_b = 0) \rightarrow O_2(v_a') + N_2(v_b' = 0)$.

kinetic energy). From the square modulus of the amplitude of the vibrational transition the detailed quantum-classical estimates of the cross section and rate coefficient can be worked out (by integrating over energy and averaging over the initial Boltzmann distribution of kinetic and rotational energies respectively) and compared with QCT ones.

The classical approximation for the rotational motion of the two colliding molecules imposes a lower limit on the gas temperature (around $T = 200$ K for the N_2–N_2 and N_2–O_2 systems). Moreover, a quantum description of the molecular rotations have a slight impact on the rate constants at the lower temperature limit. Therefore, the quantum-classical method, also known as the semi-classical coupled-state method according to the first formulation given by Billing [194] is quite accurate over a wide temperature range; this accuracy is mainly determined by the accuracy of the interaction potential. An extensive data base of state-selected rate constants [54, 195, 196] has been calculated within the quantum-classical approach for a number of diatom–diatom systems relevant to the kinetics of laboratory low-temperature/low-pressure plasmas and in aerothermodynamics. It is worth noting that the semi-classical rate constants are, quite often, taken as reference rates to check the accuracy of analytical rate constants based on first-order dynamical approximations [56]. Figure 11 compares the QCT and semi-classical methods for a set of StS rate coefficients for the $N_2 + N_2$ system (for details see [55]). One can see that semi-classical rates are in general smaller than the QCT ones (although still of the same order of magnitude) except for the quasi-resonant transition $(25; 25|24; 26)$, a case in which semi-classical values are, on average, 20% smaller. Results for the $N_2 + O_2$ system are shown in figure 12, reporting a comparison of experimental and semi-classical rate coefficients for the $O_2(v_a) + N_2(v_b = 0) \rightarrow O_2(v_a - 2) + N_2(v_b = 1)$ vibrational transitions, with v_a, the nitrogen vibrational quantum number, varying from 11 to 25. The rate coefficients are calculated using two different N_2–O_2 intermolecular PESs, denoted as GB1 [198] and MF [190]. For the N_2–O_2 system, a comparison of the semi-classical and QCT methods is provided in figure 13, which shows the rate coefficients at $T = 1000$ K calculated on the two PESs, GB1 and MF, for single and double quantum vibrational de-excitation of the process $O_2(v_a) + N_2(v_b = 0) \rightarrow O_2(v_a') + N_2(v_b' = 0)$. It can be seen that QCT results reproduce the behavior of the semi-classical rate coefficients reasonably well. Rate coefficients of multi-quantum transitions of type $O_2(v_a) + N_2(v_b = 0) \rightarrow O_2(v_a') + N_2(v_b' = 0)$, for different initial values of the O_2 quantum number $v_a = 13$, 19 and 25, and as obtained from the two potential energy surfaces GB1 and MF, are shown in figure 14.

3.3. Atom–molecule collisions

Collisions of atoms with diatomic molecules are nowadays commonly treated with approximate or 'exact' quantum mechanical (QM) methods [199, 200] or semi-classical approximations [201]. However, when dealing with application to detailed models, normally reactive and non-reactive

processes as well as dissociation/recombination have to be considered both from and to the whole sets of molecular ro-vibrational states for both reactants and products, possibly on more than one PES, in quite large collision energy ranges. In this context it is obvious to use more approximate methods, such as the Schwartz–Slawsky–Herzfeld (SSH) theory [52, 202, 203], forced harmonic oscillation [204, 205], and QCT, in order to use reasonable amounts of computational resources. QM methods can be used to assess the validity of a limited number of transitions treated with more approximate methods. However, it is important to realize that the reliability of a QM result is strongly dependent on the specific conditions and approximations in which the calculations are carried out. Even treating all degrees of freedom of the system quantum mechanically (these calculations are generally considered as 'accurate'), it is common to calculate the dynamics only for the first or very few values of total angular momentum J, using various approximations to obtain the cross sections or rate coefficients, because of the need for keeping low the computational load requirements, which increases very rapidly with J. These approximations are accurate for very low collisional energies, but for values greater than thermal energies are considered, e.g. such as those needed in aerothermodynamics, their reliability must be carefully assessed. For approximations which reduce the number of degrees of freedom, such as the infinite-order sudden approximation (IOSA [206]), which neglects, in particular, molecular rotation, it is very difficult to estimate their reliability without comparisons with accurate calculations. The role of molecular rotation is, nowadays, largely acknowledged in aerothermodynamics [23]. Even if only vibrational kinetics is often considered in most calculations, initial rotation should be at least considered as a parameter. However, if dissociation/recombination is important in a given kinetic scheme (and it is very likely that it is important for sufficiently high energy), then rotation should be explicitly considered [64]. Conversely, quasi-classical calculations tend to be more and more reliable for increasing total energy values. This means that rotational effects and dissociation can be obtained with a high level of accuracy for sufficiently high energy values. A particularly striking comparison of different quantum mechanical approximations with respect to quasi-classical results for reaction in a very light atom–molecule collisional system is presented in [207]. In that paper, different QM approaches (time-independent, wave packet and approximate ones) are compared with quasi-classical results using the same PES. While, for collisional energy less than 70 meV, the agreement is good only among QM methods (including the approximate one, but only for energies lower than 20 meV), for energy values between 0.1 and 1 eV the agreement between QCT and time- independent QM is undoubtedly the best one. In the same interval, wave packet calculations show a significant discrepancy, while the approximate QM appears to be unreliable. This is another strong confirmation that QCT can be considered the method of choice for heavy particle collision applications when sufficiently high temperatures are considered, as in aerothermodynamics.

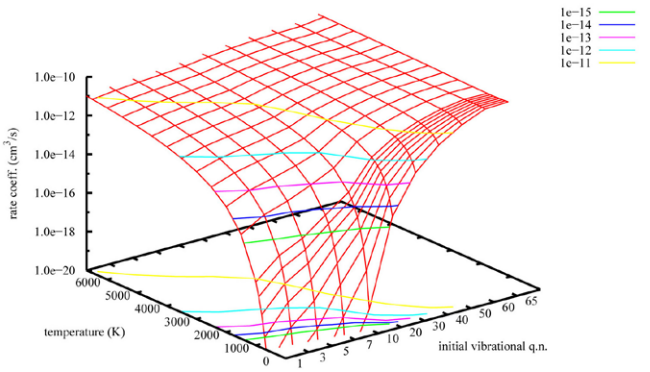

Figure 15. Mono-quantum vibrational de-excitation rate coefficients for N+ N_2 (v, $T_{trasl} = T_{rot}$) as a function of initial vibrational quantum number and ro-translational temperature [215].

3.3.1. N+ N_2. One of the most important collisional systems to consider for the modeling of aerothermodynamics is N + N_2, on which topic there is significant literature nowadays. The first PES historically available for this system was the semi-empirical LEPS PES of Laganà and Garcia [208, 209]. These authors have also calculated many vibrational transitions by means of QCT, and their results have been used in models [210, 211], after some interpolations. It is important to emphasize that in order to use data in detailed kinetic models it is necessary to have the complete network of possible transitions among the whole ro-vibrational ladder of initial and final molecules, or at least a good guess for neglecting some specific transitions. Interpolations and extrapolations to obtain missing data from an incomplete set of transitions can cause large errors in the simulations [212]. This is the reason for calculating as complete as possible set of transition rates among the initial and final ro-vibrational states. However, in the N+N_2 case one should consider almost 10 000 ro-vibrational states, so some strategy is needed for minimizing the computational effort. In [213, 214] the strategy consists of limiting the number of initial vibrational states (one in five), and considering some values of rotational temperature (allowing rotation to be considered as a parameter in simulations). In [42] all the reactants' rotational states are considered, but only about one in ten initial vibrational states. A graphical representation of the mono-quantum de-excitation rate coefficients obtained in [215] is given in figure 15, where the rate coefficients are shown as a function of initial vibrational quantum number and ro-translational temperature. It is clear that in this case the trend is quite smooth, without any special issues concerning the interpolation. In fact, rate coefficients can be interpolated on initial vibration with fairly good results, as in [42], but if cross sections are needed in the simulation, as in a direct Monte Carlo approach [216], their interpolation is much more difficult and uncertain, with large errors possible.

In [217] all the initial vibrational states are considered, but initial rotation is limited to some values. However, using data without an interpolation on rotation can cause inaccuracies. Probably the best strategy is to use a simple linear interpolation between increasing non-contiguous values of initial rotation. This approach has been tested for similar systems [94] with good results. In [49] the whole ladder of ro-vibrational

states have been considered in calculations, using a mixed approach including both some points on the energy axis for low collisional energies and some translational temperatures to distribute other points, in order to keep the computational load to a feasible level. In the cited work, a very accurate *ab initio* PES has been used [199], having a metastable N_3 state in the strong coupling region (the so-called 'Lake Eyring' feature [199]). This feature has subsequently been reproduced in other studies of the same system [218, 219]. Some preliminary comparisons between VT data obtained in [218] and in [215] including just $v = 0$, 1 initial vibrational states show that for reactive processes a discrepancy is seen and is justified by the absence of the Lake Eyring as well as by the significantly lower reaction barrier in the LEPS PES. Nevertheless, non-reactive rate coefficients appear quite similar. A detailed study (including higher vibrational states as well as dissociation) is needed to appreciate the differences between the two PESs, which cannot be expected to be completely negligible. A complete public dataset of cross sections on this accurate PES does not exist, and is not simple to obtain, because of the high computational cost of the numerical calculation. It is important to understand that from a computational point of view there are huge differences among different PESs of the same system, both in terms of purely computational problems (sometimes the numerical code of the PES is not amenable to being easily rewritten for better performance) and due to the intrinsic complexity of the dynamics involved (as in the case of the presence of the Lake Eyring, where the collisional system can spend a lot of time). This has the consequence of producing datasets of cross sections which are not optimal for modeling because of large statistical errors due the reduced set of trajectories used in order to keep the computational load to an affordable level. Computational performance in calculation of large sets of dynamical data is fundamental, and it strictly depends on the performance of the PES. This point can appear secondary when obtaining a new PES fit, with the greatest attention devoted to accuracy, but from the point of view of applications it should be carefully considered.

3.3.2. $O+O_2$. This collisional system is particularly interesting from a dynamical point of view, because of the possible formation of O_3 as a transient species during the scattering process. From a computational as well as a modeling point of view, this results in a triple drawback: the PES is quite difficult to obtain, the dynamics is generally very complicated and long [220], and simple models for data can hardly substitute true dynamical calculations. Moreover, this system also has excited electronic states lying no more than about 1.2 eV from the ground state, casting doubts on the reliability of purely adiabatic dynamics in the hyperthermal regime. In recent years, many studies have been conducted on this system including excited electronic states, but in very few cases are the PESs actually available for calculations. It should be considered that there are also significative variations among PESs of different authors, as in the case of negative or positive temperature dependence of reactive rate coefficients around room temperature, as a consequence of the absence or presence of a tiny barrier (a 'reef' structure) in the entrance and exit channels [221]. Better agreement with experiments would require a negative dependence, as found by Varandas and Pais [222] and more recently by [221] (see also dynamical results in [223]). From the point of view of modeling for aerothermodynamics, however, available data are found in [47], with a limited treatment of initial vibrational states, and from [220, 223], where both dissociation and vibration-translation (VT) rate coefficients are present from many initial vibrational states and a complete treatment of molecular rotation on the [222] PES. Suited rate coefficient interpolations in [224] give a complete treatment of the full vibrational ladder. The results are freely available in [19], with good global comparisons with experimental data. A graphical representation of available rate coefficients for vibrational mono-quantum de-excitation [220, 223] can be found in figure 16, with similar conditions to those in figure 15. From the comparison of the two figures, it is clear that the trend is completely different. The range of rate-coefficient values is less than one order of magnitude for oxygen, while in the case of nitrogen with the LEPS PES it is of many orders of magnitude. This striking difference is due to the presence of the metastable O_3 in the PES, which acts as a redistributor of vibrational energy among initial and final vibrational states. In [7] comparisons

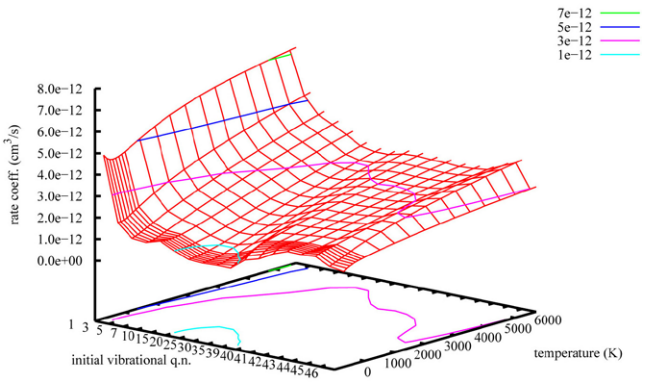

Figure 16. Mono-quantum vibrational de-excitation rate coefficients for $O+O_2$ (v, $T_{trasl} = T_{rot}$) as a function of initial vibrational quantum number and ro-translational temperature [220, 223].

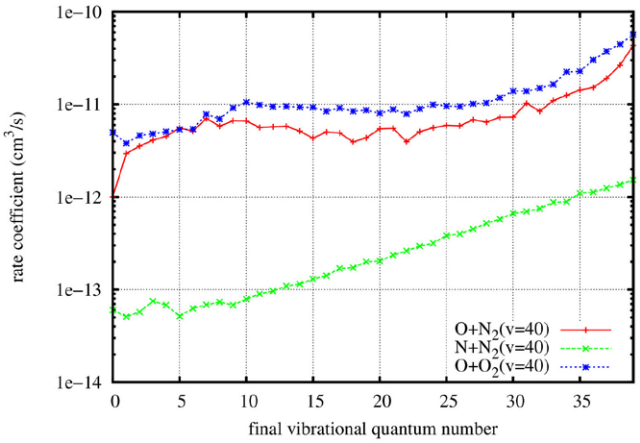

Figure 17. Comparison of vibrational de-excitation rate coefficients for the collisional systems $O+N_2$, $N+N_2$ and $O+O_2$ from the initial vibrational quantum number $v = 40$ and for $T = T_{rot} = 300$ K.

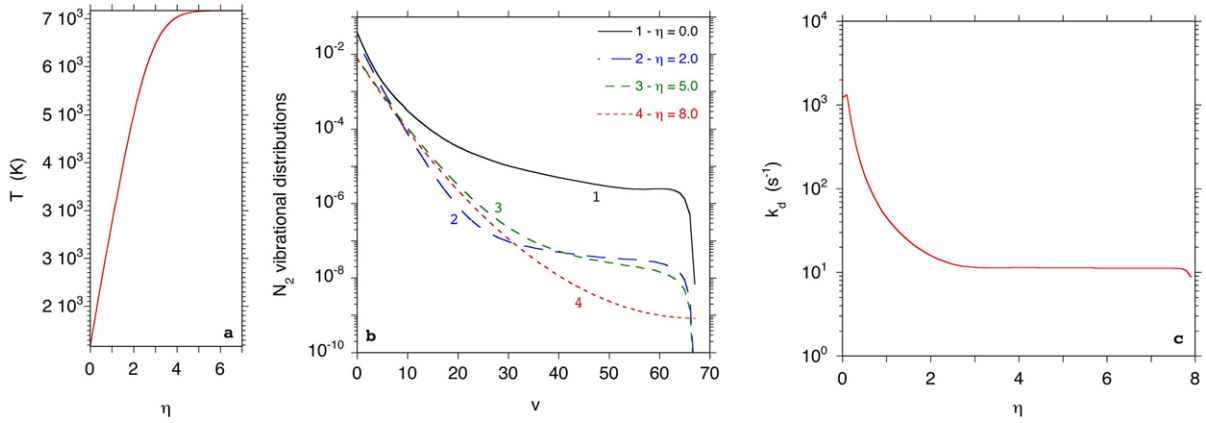

Figure 18. (a) Gas temperature T along the normal to the body surface, η, in the hypersonic boundary layer under study, (b) nitrogen vibrational distributions at different distances from the surface and (c) pseudo-first-order dissociation constants as a function of η, calculated according to the QCT model. The mixture is a N_2/N one with wall temperature $T_w = 1000$ K, edge temperature $T_e = 7000$ K, pressure $P_e = 1000$ N m^{-2}, inverse of the residence time in the boundary layer $\beta = 5000$ s^{-1} [27].

of reactive and non-reactive VT rate coefficients are shown for H+H_2, N+N_2 with a PES without the Lake Eyring feature and O+O_2. In this last case, the absence of a barrier on the Varandas and Pais PES allows quite similar behavior for both reactive and non-reactive processes, with the only difference being a clear elastic peak as a function of final vibrational state for any given initial vibrational state. Apart from this peak, the trend is almost flat for de-excitation, because of the statistical equipartition of vibrational energy due to the presence of the O_3 well, as in the preceding discussion for N_3 with Lake Eyring. While the elastic peak with quasi-elastic shoulders typical of the non-reactive part can be correctly described by simple methods based on quantum-classical correspondence of a forced harmonic oscillator, the flat trend common to reactive and non-reactive processes of this system can hardly be reproduced by these methods.

3.3.3. O+N_2. This is another very interesting collisional system for which few detailed calculations are present in literature. The reaction to form NO is endothermic by more than 3 eV, so calculations have been generally performed in the opposite direction to benefit from higher probabilities. One notable exception is [44], where quasi-classical and wave packet calculations are compared with good results for sufficiently high total energy, as expected. The features of the two accurate uncoupled triplet PESs used are dynamically studied, with interesting effects due to the presence of metastable states in the strong coupling region (SCR). These effects can also be stressed by comparing different collisional systems from a given initial vibrational state, $v = 40$ in figure 17, where the vibrational energy exchange rate coefficient is shown as a function of final vibrational quantum number for O+N_2, N+N_2 and O+O_2, in the non-reactive case. While for N+N_2 the LEPS PES is adopted (without any metastable state), in the other two cases the presence of a minimum in the SCR deeply affects the final vibrational distribution of probabilities, with a clear tendency to a flat trend (except the elastic peak and its shoulders). A more complete work on this system is in preparation by some of the present authors, with a very detailed database of both VT and dissociation. Some preliminary results have been presented in [94]. The non-reactive process, however, shows important issues. The comparison with experimental data is acceptable only for temperatures higher than 4000 K, while twenty orders of magnitude of discrepancy can be found at room temperature. It is very likely that for intermediate regimes of temperature it is necessary to investigate to what extent this issue can affect aerothermodynamical models. However, this investigation is not free from serious difficulties. In [225] it is shown that, while quasi-classical trajectories are unable to reveal any inelastic transition at room temperature (it is a 'classically forbidden' process [226]), a quantum approximate calculation is able to give a non-zero rate coefficient, but too low to be in quantitative agreement with experimental values. As also suggested from those authors, a more accurate study should include a non-adiabatic spin-forbidden transition from the triplet surfaces correlating with O+N_2 in their respective ground states to the singlet PES of N_2O. The formation of a long-lasting complex on this surface with final exit on the triplets could have the effect of a flat vibrational distribution in products, which could explain the large VT rate coefficients in the experiment. This investigation requires the singlet surface of N_2O, the couplings with the two triplets of O+N_2, and the treatment of non-adiabatic transitions both by a classical method as well as a semi-classical or approximate quantum method, in order to better understand the nature of the effect.

3.4. Atom–molecule collisions: applications

The availability of a very accurate and complete set of QCT StS rate coefficients, including dissociation rates, allows one to obtain more precise results in many aerospace applications including the hypersonic boundary layer. In the past, the ladder climbing (LC) dissociation model has been widely used [5, 68, 211, 227]. LC adds to the bound levels of the vibrational ladder a pseudo-level located just above the last bound level i.e. in the continuum. In turn the dissociation rate is calculated by extrapolating the bound–bound VV and VT rates to the pseudo-level. In a N_2/N mixture, the large differences

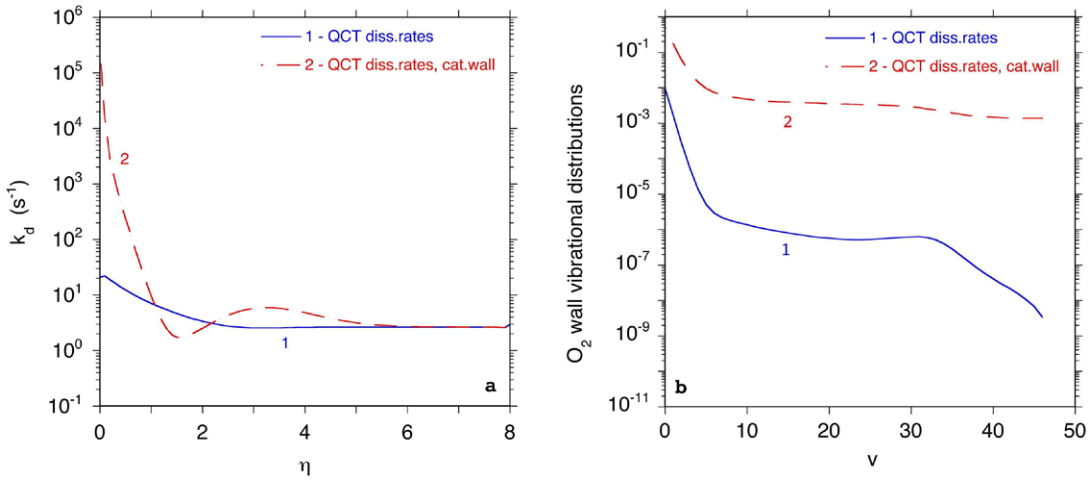

Figure 19. (a) Pseudo-first-order dissociation constants as a function of η in the hypersonic boundary layer under study and (b) wall oxygen vibrational distributions calculated according to the QCT model both in the case of a non-catalytic surface and in the case of a partially catalytic one. The mixture is an O_2/O one with $T_W = 1000$ K, $T_e = 4000$ K, $P_e = 1000$ N m^{-2}, $\beta = 5000$ s^{-1}. The heterogeneous recombination coefficients are from reference [69].

between the results obtained by using QCT rates and LC ones are observed in the hypersonic boundary layer flows as well as in nozzle-expanding flows [27, 228]. In the following, only results obtained with the QCT model (figures 18 and 19) will be reported. In the boundary layer flows the gas temperature strongly decreases from the edge of the boundary layer ($\eta = 8$) to the surface ($\eta = 0$) (figure 18(a)) promoting the corresponding dissociation-recombination kinetics and creating non-Boltzmann vibrational distributions (figure 18(b)). In this figure we can observe a plateau in the vibrational distribution at different distances from the surface η resulting from the preferential pumping of vibrational levels by the recombination process. These non-equilibrium vibrational distributions generate an anti-Arrhenius behavior of the dissociation constant versus η in the region $0 < \eta < 2.5$ (figure 18(c)) i.e. the dissociation constant increases, decreasing the gas temperature.

Similar results have been obtained for the N_2/N/O_2/O/NO mixture where the different QCT rates reported in this review have been used [26]. In addition, results for the CO_2/CO/C/O_2/O mixture relevant to Mars entry aerothermodynamics can be found in [70, 88, 229].

Another case study deals with non-equilibrium in boundary layer kinetics of an O_2/O mixture [28] for partially catalytic and non-catalytic surfaces. In the case of partially catalytic surface, the molecular dynamics results presented in section 4, which show the preferential pumping of vibrational levels during the heterogeneous recombination, were used. In figure 19 the pseudo-first-order dissociation rate as a function of η (figure 19(a)) and the vibrational distributions close to the surface (figure 19(b)), obtained considering either a non-catalytic surface or a partially catalytic one [69] are reported. The results emphasize the importance of using molecular dynamics methods either for the gas phase or for the gas surface interaction.

3.5. The prototypical case of CO_2 plasmas

Large theoretical and experimental interest is presently dedicated to the activation, i.e. dissociation, of CO_2 under cold plasmas as well as in aerospace technology (Mars entry problems as well as propellant in helicon electrical thrusters). In both cases, the dissociation process stimulated by vibrational excitation plays an important role, implying a strong effort in the corresponding theoretical characterization. Pure vibrational mechanisms versus mechanisms induced by direct electron impact have been recently reconsidered in the case of N_2 and CO plasmas [24]. In this section, we discuss the same mechanisms for CO_2 molecules, stressing the most important cross sections acting in the system. In CO_2 plasmas, especially at low electron temperature ($T_e \leqslant 2$ eV), the input of electrical energy goes through the excitation of vibrational modes of CO_2 (in particular the asymmetric one) followed by VV energy exchange processes able to spread the low-lying vibrational quanta over the whole vibrational ladder of CO_2, ending in the dissociation process. The upper limit to the pure vibrational mechanism can be obtained by the simplifying equation (13) [24]

$$K_d^{\text{ulPVM}} = \frac{1}{v_{\max}} k_{\text{eV}}(0 \to 1) \tag{13}$$

where $k_{\text{eV}}(0 \to 1)$ is the rate of the resonant $(0\,0\,0) \to (0\,0\,1)$ vibrational excitation process and $v_{\max}$ the number of vibrational quanta contained in the vibrational ladder of CO_2. Equation (13) assumes that the vibrational quanta on the asymmetric vibrational ladder of CO_2 introduced by electron–molecule resonant processes are transported by a VV up-pumping mechanism to the dissociation continuum. This rate can be several orders of magnitude higher than the corresponding dissociation process induced by electron impact from the ground state [95]. The calculation of equation (13) requires the knowledge of the cross sections for the resonant vibrational excitation process

$$CO_2(000) + e \to CO_2^- \to CO_2(001) + e \tag{14}$$

as well as a Boltzmann solver to get the eedf of the cold plasma. The Boltzmann solver should contain elastic, inelastic, dissociation, ionization and superelastic cross sections of the CO_2. One of the most used databases for CO_2 is that one compiled

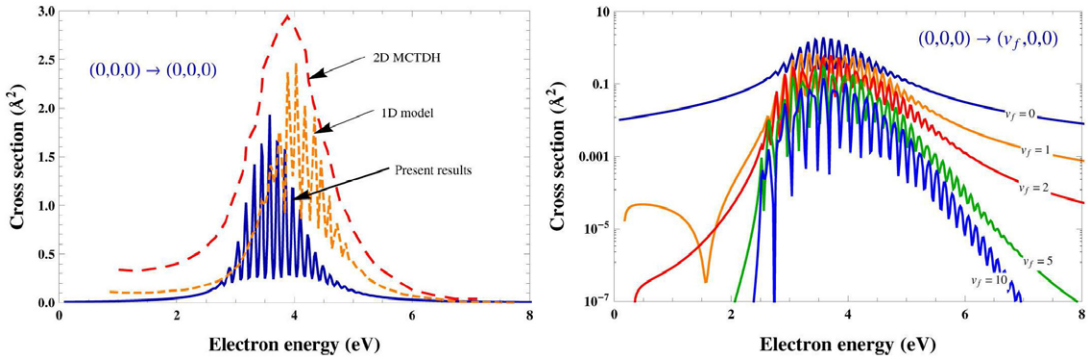

Figure 20. (left) Elastic electron-CO_2 resonant cross section: 1D results of Laporta *et al* [91] (solid line) compared with 1D boomerang model (short-dashed line) and MCTDH (long-dashed) from [235]; (right) electron-impact resonant excitation of CO_2 symmetric modes, $(000) \rightarrow (v_f 00)$, for different values of the final symmetric vibrational quantum number [91].

by Phelps [230, 231] referring to the interaction of electrons with $CO_2(000)$. In particular, the Phelps database contains resonant vibrational excitation transitions over the other vibrational modes of CO_2, including some combined levels. Use of the Boltzmann solver with the reported cross sections allows us to calculate K_d^{ulPVM} and to compare it with the corresponding direct dissociation rate $K_d(v = 000)$, i.e. of the process

$$\mathrm{CO_2}(0\,0\,0) + e \rightarrow \mathrm{CO} + \mathrm{O} + e \tag{15}$$

The comparison as a function of E/N in the presence or absence of superelastic vibrational collisions confirms, at least for $E/N < 50$ Td, the old hypothesis, i.e. $K_d^{\mathrm{ulPVM}} > K_d(v = 000)$ [95]. The accuracy of the different rates can hopefully be estimated to one or two orders of magnitude, this (in)accuracy reflecting the incomplete sets of electron–molecule cross sections and influencing the eedf (and in turn the rates of electron-impact-induced processes). To understand this point, [95, 232, 233] the hierarchy of the different rates have been recalculated by introducing in the Boltzmann solver all the vibrational excitation cross sections linking the asymmetric ladder, calculated by using the scaling law of Fridman [234]. The results show that this addition of cross sections, while not affecting the hierarchy of rates, strongly affects the absolute values of electron-impact dissociation rates through changes in eedf. A similarly strong influence should be expected if one introduces into the Boltzmann solver all eV transitions including the different modes of CO_2, i.e. the processes:

$$\begin{aligned}
&\mathrm{CO_2}(v00) + e \rightarrow \mathrm{CO_2^-} \rightarrow \mathrm{CO_2}(w00) + e \qquad \text{symmetric}\\
&\mathrm{CO_2}(0v0) + e \rightarrow \mathrm{CO_2^-} \rightarrow \mathrm{CO_2}(0w0) + e \qquad \text{bending}\\
&\mathrm{CO_2}(00v) + e \rightarrow \mathrm{CO_2^-} \rightarrow \mathrm{CO_2}(00w) + e \qquad \text{asymmetric}
\end{aligned} \tag{16}$$

An attempt in this direction has been undertaken by Laporta *et al* [91] by considering the independent vibrational modes of CO_2. The resonant cross sections and the corresponding rate coefficients for electron-CO_2 scattering were studied in the framework of the R-matrix method [155], by considering the normal mode approximation. The potential energy surface of the ground electronic state of CO_2 was obtained by MOLPRO [166], an *ab initio* quantum-chemistry package. In both calculations the cc-pvQZ basis and the MRCI model were used. Some cross section results are shown in figure 20.

Coming back to equation (13), we must emphasize that this equation gives only the maximum contribution of a pure vibrational mechanism in the absence of any VV and VT energy transfer processes. The situation may be largely improved by solving an appropriate vibrational master equation for the three modes of CO_2 [88, 236, 237]. A lot of problems arise in this description, the most important of them being the calculation of complete data set for VV and VT processes occurring in the system. Complete sets of VV and VT rates can be calculated by the SSH theory scaling through corresponding theoretical values over the lower vibrational levels. More recently, Lombardi *et al* [191] have obtained a set of VV and VT rates by running QCT on an accurate PES. The master equation used by Armenise and Kustova [88] covers conditions where vibrational excitation affects the dissociation recombination regime in hypersonic flows without considering the presence of electrons. Neglecting the electron–molecule collisions is the weak point of this model that needs to be overcome. Unfortunately, insertion of this accurate model into a non-equilibrium plasma kinetics scheme is sometimes prohibitive due to the number of excited levels. In this sense, the vibrational master equation developed by Bogaerts *et al* [237], describing the asymmetric mode linked to the other modes by some intermode VV and VT energy transfer reactions, is an attempt to investigate the vibrational state of the CO_2 molecule with a reduced vibrational model. Again, the set of VV and VT rates are scaled by using the SSH theory and some experimental and theoretical values of the low lying vibrational levels. The accuracy of these rates can, once more, be checked against the QCT estimates of Lombardi. In the Bogaerts *et al* [237] vibrational kinetics an effort is also made in relation to the role of vibrational excitation in affecting the dissociation rates of CO_2 by heavy particle collisions. They use a kinetic approach essentially based on the absolute theory of chemical reactions where vibrational excitation decreases the activation energy of the process. Of course, QCT calculations can be a further improvement on the process provided the PES for VV and VT rates by Lombardi *et al* [191] is used and allow the addition of reactive channels and further checks by comparison with quantum-classical results.

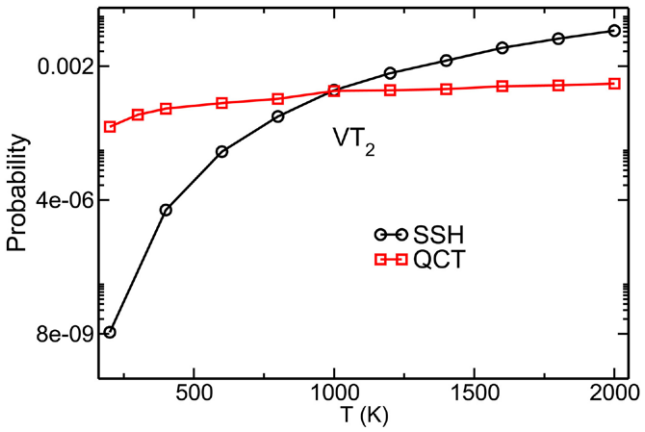

Figure 21. The VT_2 probabilities are shown as a function of temperature and compared with the corresponding results from SSH theory [236].

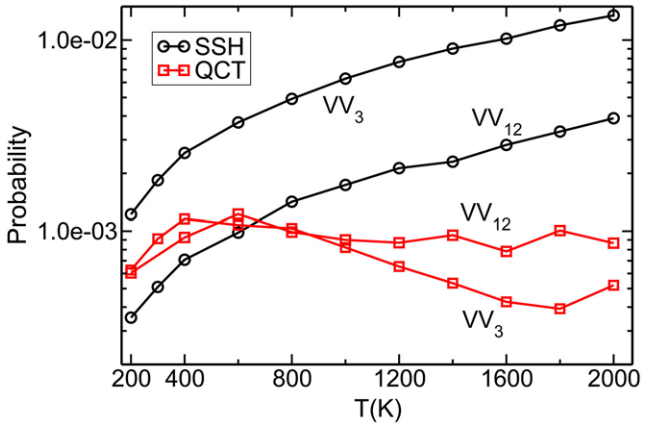

Figure 22. The VV_{12} and VV_3 probabilities, as a function of temperature, obtained from QCTs are compared with the corresponding results from SSH theory [236].

Energy exchange probabilities obtained by QCT are shown in figures 21 and 22 for VV and VT processes as a function of the temperature T and compared with the corresponding values from the SSH theory from [236]. Figure 21 shows the probability of VT_2 energy exchange (vibration-translation exchange involving a quantum of bending vibrational energy). According to the classification provided in [236], VT_2 processes are as follows:

$$CO_2(v_1, v_2, v_3) + M \rightarrow CO_2(v_1, v_2 \pm 1, v_3) \qquad (17)$$

where v_2 is the quantum number of the doubly degenerate bending mode of CO_2. Figure 22 shows the QCT energy transfer probabilities as a function of the temperature T for VV_3 and VV_{12} vibration–vibration exchange processes, where, according to the classification proposed in [236], a quantum of energy of asymmetric stretching goes from one to another of the colliding CO_2 molecules (VV_3) and a quantum of energy of the symmetric stretching goes into the bending mode (VV_{12}, intramolecular energy transfer). To obtain the VT_2 and VV_3 thermal probabilities, a batch of ~7 million trajectories has been run, with initial vibrational state (0, 0, 1) + (0, 0, 0) and temperatures ranging from 200 to 2000 K. The choice of such an initial vibrational state of the molecules permits one to directly calculate VV_3 rates (here, presented as probabilities to be compared with SSH results) and to give an estimation of the VT_2 rates, measuring the probability of the transfer of energy from translations to the bending mode of CO_2. A different, smaller set of trajectories, with initial vibrational states (n, 0, 0) + (0, 0, 0), $n = 1, ..., 5$, has been used to obtain an estimation of the VV_{12} processes probability in the given temperature range. Marked differences can be seen to exist between QCT and SSH probabilities, especially for the VV_{12} and VV_3 processes at temperatures higher than 800 K. This can be, in part, due to the sensitivity of the QCT StS results to the initial vibrational states. However, the deep causes of such disagreement can be numerous, and have to be sought in the approximations underlying the SSH theory, which may compromise the capability of the theory to provide correct results, or, on the other hand, in some degree of arbitrariness always present in the procedure adopted to quantize the classical final vibrational states in the QCT method. Experimental data, mostly lacking, would be extremely useful for validation.

4. Gas-surface processes

The catalytic properties of surfaces can be studied in a very detailed way by the MD simulations that enable the description, at atomic level, of the elementary processes due to the interaction of gaseous species (atomic or molecular) with solid surfaces. These processes include atomic and molecular adsorption (sticking), elastic and inelastic scattering, recombination (ER, LH and HA) and molecular dissociation. In particular, the recombination process is an effective source of ro-vibrationally excited molecules and, at the same time, is effective for surface atom abstraction and atom/molecule removal from the plasma region [67]. Moreover, adsorbed species, the initially adsorbed species or the new-formed molecules, will desorb. On the other hand, two additional homogeneous processes, diffusion of reactants onto the surface and diffusion of products away from the surface will also occur. ER and LH processes will compete depending on the experimental conditions. Commonly, the LH mechanism will be more favorable at low temperatures due to the high surface coverage. At higher temperatures, with a much lower coverage, ER and HA mechanisms will become more important, unless the mobility of adsorbed species is high.

Adsorption processes and recombination reactions will be exothermic processes which are more important than the endothermic desorption processes, hence producing an overall heat release to the surface. This heat flux is in addition to molecular conduction and can achieve up to 40% of the total heat flux inside the stagnation region. Thus, TPSs should be poor catalytic materials (e.g. silica-based materials) and characterized by high emissivity and low thermal conductivity. In contrast, ablative TPSs can accommodate high heat fluxes through phase change and mass loss [238–240].

The exothermicity partitioning process is controlled by several molecular and surface parameters as, in particular, the collisional mechanism that is behind the recombination reaction, the active surface sites involved in the interaction,

and, therefore, the nature, coverage and temperature of the substrate, and the dynamical coupling between atoms/molecules and the surface. The number and complexity of these effects is evidently high. Indeed, this issue, i.e. the energy-sharing mechanism in chemical surface processes, is among the most complex and intriguing problems relevant to re-entry condition simulations. In fact, predictions of the TPS catalytic response made in various space missions have failed due to the insufficient knowledge of the exothermic processes that can be active at the shuttle walls.

The predictive character of advanced kinetic models of the boundary layer [69, 241] in estimating the heat flux to the TPS tiles relies on the knowledge of: (1) StS recombination probability, $P_i(v|E_{kin})$, i.e. the probability that i-atom or molecule recombines at the surface forming a molecule in v vibrational level for a given collisional energy, E_{kin}; (2) global and state-selected recombination coefficient, $\gamma_i(T_S)$ and $\gamma_i(v|T_S)$, i.e. the fraction of total atoms (or molecules) in the incoming flux that ends in molecular form and in a given vibrational quantum number, v, after colliding for a given surface temperature, T_S; (3) energy accommodation coefficient, $\beta_i(T_S)$, the ratio of energy released to the surface per atomic recombination to the maximum energy transferable; (4) the molecular vibrational distribution into the final states, N(v), the probability that molecules form in a given vibrational quantum number; (5) state-selected dissociation probability, $P(E_{kin}|\{.\}|v,j|T_S|)$, the probability that a molecule in (v, j) ro-vibrational levels, dissociates.

The lack of a collisional database of heterogeneous processes, except for the recent database Phys4Entry [19], is mainly due to the fact that surface processes are very specific. In fact, the sticking coefficient S, as well as the recombination coefficient γ_i depend upon some molecular behavior, such as the internal energy state, impact energy, orientation angles, etc. of the reactants, but also upon the chemical-physics properties of the surface: structural and chemical composition, corrugations, coverage, which are strictly correlated to the conditions of the plasma environment. The determination of these surface parameters in real systems under operative conditions is obviously not an easy task.

Several studies concerning elementary surface processes occurring in Earth, Jupiter and Mars atmospheres with two materials, silica (β-cristobalite and β-quartz) and graphite that can be used as material models of real TPSs have been performed by some of the present authors. These surfaces are exposed to molecular oxygen, hydrogen, nitrogen and CO_2 fluxes, due to the interest for these molecules and their dissociation species in relation to entry in Earth, Jupiter and Mars atmospheres. In spite of the major abundance of N_2 molecules compared to O_2 molecules in air, the much lower O_2 dissociation energy favors the atomic oxygen formation during re-entry conditions and hence the O adsorption and the subsequent atomic recombination will become the most important elementary process in Earth atmosphere.

4.1. Oxygen, nitrogen, hydrogen and carbon oxide

In the pioneering paper concerning the recombination of oxygen atoms on a silica β-cristobalite surface [76], a switching of the reaction mechanism from ER to LH with the surface temperature decrease was pointed out. This result was stated by comparing the recombination coefficient obtained from MD simulations at different T_S with the corresponding experimental data available for O atom recombination on silica or silica-like surfaces. In another study [75], oxygen atom recombination on β-quartz was studied showing that, despite the common tetrahedral structure, the different binding configuration of the SiO_4 tetrahedra gives rise to a different catalytic activity of the two polymorphs. The paper also gave a validation of semi-classical collisional method [242, 243], used in MD simulations, because a good qualitative and quantitative agreement was obtained between the theoretical and the experimental recombination coefficients in a wide range of surface temperatures. Evidence was also given of the higher catalytic response of cristobalite with respect to the quartz surface toward the O atom recombination (γ_O (β-cristobalite) $> \gamma_O$ (β-quartz)).

Some years later, another study of atomic gas oxygen colliding with a clean β-cristobalite surface [244] was carried out by using classical trajectories for normal and off-normal incidence, 0.1–1 eV collision energies and surface temperatures between 300 K and 1100 K. The large adsorption energy for O over top Si atoms seems to play a key role in the dynamics of the sticking process; this is mainly produced via the absorption/penetration of O into the SiO_2 slab instead of a simple adsorption. To see the effect of oxygen coverage in the O sticking process, which also competes with the ER reaction to produce O_2, a similar DFT-based PES was developed for the O + O/β-cristobalite system [72, 245]. Classical trajectories were calculated for 0.01–4 eV collision energies, several incident angles and surface temperatures between 100 K and 1500 K, with an O-pre-covered β-cristobalite surface. Atomic sticking was the principal process, while O_2 formation with the molecule finally adsorbed over the surface which was the second one. Atomic oxygen reflection and ER reaction (i.e. $O_{2_{gas}}$ formation) were much less important although still significant. The new O_2 molecules produced by the ER reaction at high temperatures become internally and translationally excited, while the slab becomes colder. In order to evaluate all competitive heterogeneous processes occurring for an O/O_2 gas mixture reacting on a silica surface, with different contributions to the global heat released to the surface, a microkinetic model was developed [73] for this system including ten surface elementary reactions, among them the ER and LH processes. This study allowed the determination of the atomic recombination coefficient γ_i and the chemical energy accommodation coefficient β_i. In this study, thermal rate constants were derived from previous QCT data of the forward processes or using the principle of detailed balance for reverse ones, in a wide range of temperatures (700 K–1700 K). The computed γ_O mainly had contributions from the atomic sticking and ER recombination, being very small ($0.01 < \gamma_O < 0.02$) and increasing with temperature, following an Arrhenius equation in agreement with experimental data (figure 23). In the same temperature range, an estimation of β_O was obtained, the main contribution arising from the atomic sticking process instead of the ER or LH processes,

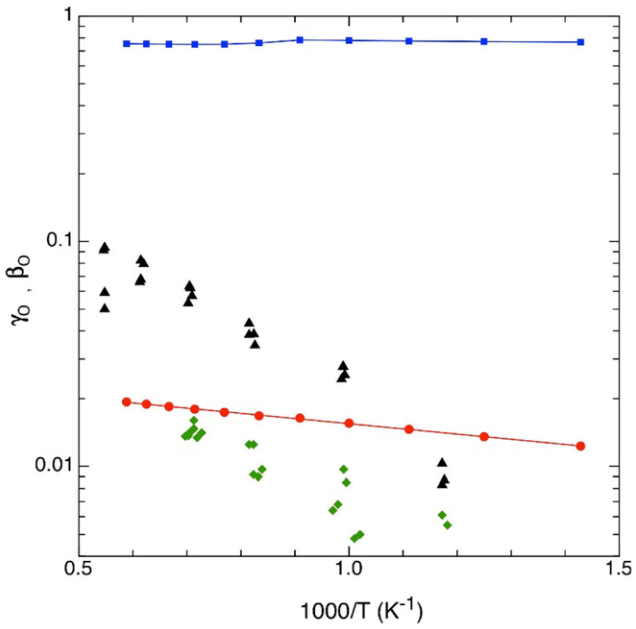

Figure 23. Calculated $\gamma_O(T)$ (red circles with a least squares fitting line) and $\beta_O(T)$ (blue squares with a simple line joining the points) coefficients versus the reciprocal of the temperature for an O/O_2 reactant mixture ($P_O = 91$ Pa, $P_{O_2} = 9$ Pa) on β-cristobalite [73]. Some experimental values for $\gamma_O(T)$ in air on β-cristobalite (black triangles) and quartz (green diamonds) at 200 Pa [246] are presented for comparison.

with an almost constant value ($0.75 < \beta_O < 0.80$), but different from the unity value assumed in earlier studies.

Using a cluster approach, the interaction potential of atomic and molecular oxygen on β-cristobalite and β-quartz was determined via density functional theory (DFT) calculations in [78, 79], where the oxygen adsorption dynamics on β-cristobalite and β-quartz were studied. It transpires that the binding energy for the gas-phase O atom interacting on the Si atom on the surface is almost the same for the two silica polymorphs, about 5.6 eV. On the contrary, interaction potential of a gas-phase oxygen interacting with the silica oxygen below the topmost Si atom layer is considerably different for the two silica polymorphs, around 2.0 eV and 1.0 eV for cristobalite and quartz, respectively. The obtained PES was inserted in the semi-classical model [242, 243] to study the adsorption dynamics for oxygen atoms on the two silica surfaces. The adsorption and inelastic scattering probabilities and the energy transferred to the surface in these two processes were determined in a large collisional energy regime, 0.05 eV $< E_{kin} <$ 0.8 eV. The probability for atomic adsorption and inelastic scattering is almost the same for the two silica polymorphs, while the energy transferred to the surface in the adsorption processes is considerably higher in the case of quartz. This last result would indicate that surface thermal damage should be more effective in the β-quartz as a result of an efficient chemical conversion scheme that funnels the kinetic energy of the impinging oxygen atom into the surface structure itself.

Using a later and more accurate PES, new MD simulations for oxygen atom recombination on β-cristobalite via the ER mechanism [82] were presented. The updated recombination

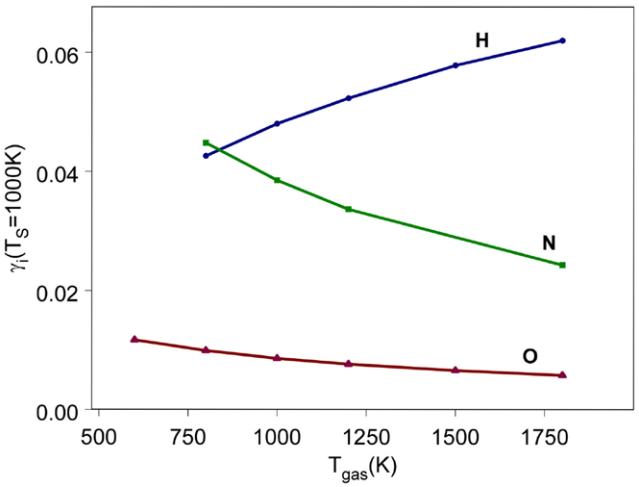

Figure 24. Recombination coefficients γ_i for H, O and N on β-cristobalite, as obtained in [80–82].

coefficients compare well with those reported in [72] and with the experimental data reported in [247]. It is worth noting that, as evident in figure 6 of [82], the experimental recombination coefficient γ_O reported in the literature as a function of the gas temperature and the surface temperature exhibits a large spread due to the different conditions of the catalytic system considered in the experiments and in the simulations. The new calculations [82] confirm the non-Boltzmann behavior of vibrational distributions of the O_2 molecules formed in the ER atom recombination reaction: at low E_{kin}, the distributions exhibit a sharp peak for $v = 0$ followed by a large band centered around $v = 20$. At higher E_{kin}, the vibrational distributions are broader with more than a maximum.

In [80] a very accurate PES, based on *ab initio* electronic structure calculations, was obtained as a first step to characterize the dynamics of nitrogen atom recombination on a silica surface. In particular, the N/N_2 interaction with a Si atom on silica model clusters was studied by calculating the interaction potential of the $N(N_2)$-SiO_2 system along the C_2 (C_{2v} molecular) symmetry axis by keeping the SiO_2 geometry fixed at the experimental values of the β-cristobalite unit cell. The more realistic N/N_2-$Si_xO_yH_z$ heterogeneous system of the β-cristobalite was also considered and the corresponding calculated interaction potential was assumed in the MD simulation of the ER recombination reaction of N atoms on the silica surface. The calculated γ_N was 0.04, while the energy transferred to the surface was nearly 40% of reaction exothermicity, mainly for low collisional energy, while at higher values of E_{kin} nitrogen molecules are formed with high translational energy. The energy partitioning of the exothermic energy released in the recombination reaction between the internal degrees of freedom of the formed N_2 molecules (vibration, rotation, translation) and the surface, shows that the recombination process promotes the population from the bottom of the vibrational ladder with a maximum peak at $v = 0$.

The dynamics of hydrogen atom recombination on β-cristobalite has been studied in detail in [81] using the semi-classical MD approach and a potential energy surface, based on DFT calculations (see [248] for details). The probabilities

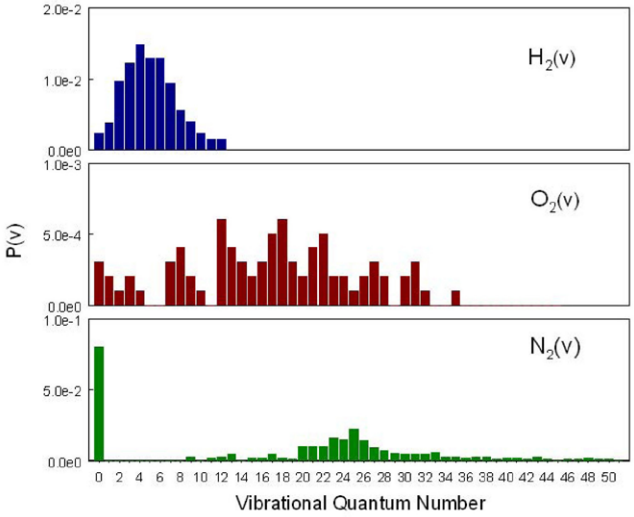

Figure 25. Vibrational population distributions of the H_2, O_2 and N_2 molecules formed on a silica surface for $E_{kin} = 0.05$ eV, $T_S = 1000$ K.

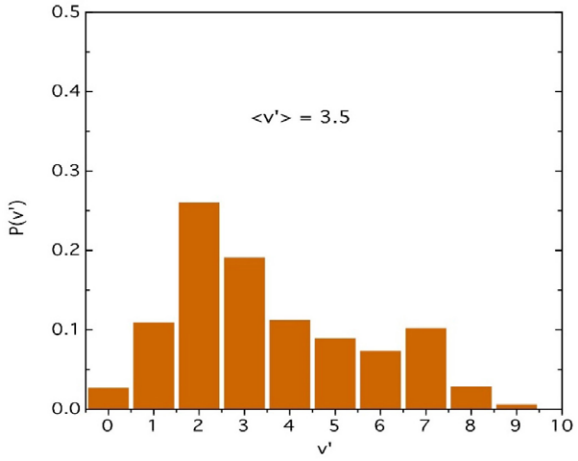

Figure 26. QCT final vibrational CO(v') distribution of reflected CO($v = 2, j = 0$) molecules colliding over an O-precovered β-cristobalite surface for normal incidence, $E_{kin} = 0.5$ eV and surface temperature of 300 K. The distribution shown is normalized to population unity. Average final vibrational value is also indicated.

for the different atomic and molecular surface processes were determined as a function of several parameters: surface temperature (300 K and 1000 K), kinetic energy (0.04–3.0 eV) and incident angles (0°, 45°) of the gas-phase H atom impinging on the silica surface. The atomic recombination dynamics was studied in detail by determining the energetics and the ro-vibrational distributions of the formed H_2 molecules obtained for the different dynamics conditions. The recombination coefficients were also obtained for the different initial conditions. In figure 24 the recombination coefficients, γ_i, for $T_S = 1000$ K for H, O and N recombination on a β-cristobalite surface are reported for comparison [80–82]. It appears that for O and N recombination γ_i decreases as the gas temperature increases, the contrary occurring for H recombination. Overall, the γ_O is the lowest coefficient in the complete range of considered gas temperatures.

In figure 25 the vibrational population distributions for H, O and N atom recombination on a silica surface for $E_{kin} = 0.05$ eV and $T_S = 1000$ K as obtained in [80–82] are reported. Looking at the figure, we can immediately infer the non-Boltzmann behavior of vibrational distributions, in particular in the case of nitrogen molecules which recombine mainly in the lowest vibrational level.

Other important series of studies have also been performed for O/O_2 reactant mixtures over a graphite basal surface, which was taken as a model for carbon-based TPSs. A first study [249] used DFT calculations to characterize all stationary points (i.e. minima and transition states) involved in the different heterogeneous elementary processes. Atomic sticking was an activated process, whose energy barrier decreased for lower coverage and under slab relaxation. The O adsorption was mostly produced on C-C bridge sites with a considerable puckering of these carbon atoms. Oxygen recombination via ER and LH mechanisms was also an activated process although their energy barriers decrease with coverage increment, especially for the ER reaction, which dominates the atomic recombination reaction from low to high temperatures because of its much lower energy barrier. The application of a microkinetic model with six elementary processes and thermal rate constants derived using the transition state theory (TST) showed a very low oxygen recombination coefficient ($\gamma_O < 5 \cdot 10^{-4}$) within the interval 300 K–900 K. Moreover, it was confirmed a very small contribution from the LH reaction and a very low atomic coverage, which along with the small rate constants, allow one to explain the low atomic recombination coefficients arising mainly from the ER reaction.

Classical dynamics studies for O [74, 250] and O_2 [251] over clean and O-precovered graphite surfaces were also made with analytical PESs based on DFT data with different collision energies (0.01–2 eV), surface temperatures (100 K–900 K) and incident angles (0°, 45°). In the first case, it was verified that atomic sticking occurs predominantly over bridge sites with low probabilities, in agreement with previous study [249]. The analysis of the distributions of the energy transferred by the reflected atoms to the surface indicated a significant release from the colliding atom to the surface, which was more important for higher atomic collision energies. The collision of O over an O-precovered graphite surface [74] indicated that ER reaction and O reflection were the main processes in agreement with earlier experimental and theoretical studies [249], becoming the ER mechanism more important than the O reflection for normal incidence and with an opposite behavior for off-normal incidence. Moreover, molecular oxygen formed via ER reaction was translationally and internally excited. Finally, the QCT study of molecular oxygen colliding over a graphite surface for some ro-vibrational O_2 levels ($v = 0$, 1, 2 and $j = 1$, 17, 25) [251] presented only O_2 reflection (even at high collision energies and vibrational excitation) in agreement with the low expected molecular dissociation. The reflected molecules lose mainly collision energy (i.e. not internal), which is primarily transferred to the surface. The calculation of γ_O and β_O coefficients for an O/O_2 gas mixture reacting over graphite could also be done in a similar way as

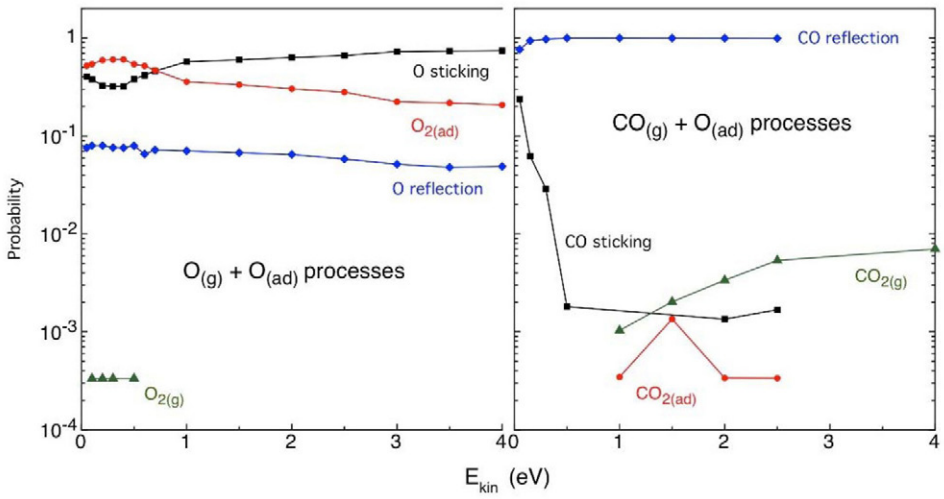

Figure 27. QCT reaction probabilities for an O-precovered β-cristobalite surface at several collision energies, with normal incidence and at surface temperature of 300 K for two gas species: (a) O and (b) CO($v = 0, j = 0$).

for β-cristobalite [73] by using the dynamical data instead of TST data obtained for the different aforementioned studies on the elementary processes, but remains missing. This study supported that O + O processes should be much more important than CO + O ones over silica-based surfaces for similar initial conditions of reactants, whose principal processes (O sticking and O_{2ads} formation) can predominantly release their energy to the surface (figure 27). The Mars atmosphere contains about 95% carbon dioxide and, during the entry of space vehicles into this atmosphere at high collision energies (i.e. about 4.5 ± 1.0 eV), it mainly produces the breaking of CO_2 molecules into CO + O. Experimental investigation into carbon monoxide and oxygen mixtures on quartz seems to indicate that oxygen recombination should be more important than CO oxidation in the range of pressures and temperatures studied [252]. On the other hand, CO molecules can react over an O-pre-adsorbed silica surface to produce atomic reflection and adsorption along with CO_2 formation, probably via an ER recombination mechanism that should be more likely than an LH mechanism. A recent study has been performed to ascertain the importance of the CO + O elementary processes in comparison with the O + O ones to shed light on this point [93]. A QCT study was carried out in this work for carbon monoxide collisions over an oxygen pre-adsorbed β-cristobalite surface by using a based reactive force field (ReaxFF) PES. The collisions were performed by fixing several initial conditions: CO ro-vibrational states ($v = 0$–5 and $j = 0$, 20, 35), collision energies (0.05–2.5 eV), incident angles (0°, 45°) and surface temperatures (300 K and 900 K). The main elementary processes were the molecular reflection and the non-dissociative molecular adsorption (sticking). CO_2 molecules were also formed in a minor extension via an ER mechanism although some of them were finally adsorbed on the surface. The scattered (reflected) CO molecules were translationally colder and internally hotter (rotationally and vibrationally) than the initial ones. The effect of the initial collision energy on these CO(v') final distributions was small, which shows a bimodal shape for initial CO molecules with $v > 2$ and for all collision energies studied (figure 26).

5. Conclusions and perspectives

The relevance of advanced StS kinetic models, including accurate and detailed dynamical information, in the reliable description of non-equilibrium conditions characterizing high-speed entry in Earth's atmosphere is well-assessed nowadays in the modeling community. A predictive theoretical model could assist the design of TPS and the choice of new materials, based on the fundamental knowledge acquired from the role of excited species in plasma in the shock region, on the catalytic response of surfaces and on the microscopic collisional mechanisms driving the plasma evolution. The StS approach has triggered intense research activity aimed at the theoretical investigation of the molecular dynamics of the elementary processes relevant to the plasma kinetics which, dealing with complete datasets ro-vibrationally resolved and in some cases also with processes involving electronically excited species, benefits significantly from the possibilities offered by modern web-access databases for the collection, validation and distribution of dynamical results. This review focuses on the most recent efforts in the derivation of accurate, complete and consistent state-resolved cross sections and rate coefficients for inelastic and reactive channels, belonging to the four main classes of processes, namely electron–molecule, atom–molecule, molecule–molecule and atom/molecule–surface, and involving the chemical species relevant to Earth (N_2,O_2,NO), Mars (CO_2,CO,N_2) and Jupiter (H_2,He) atmospheres.

The creation of this new database for the modeling of re-entry conditions in planetary atmospheres can be regarded as a step forward in the actual practicability of StS kinetics, and in understanding the role of the collisional dynamics in affecting the macroscopic quantities characterizing the plasma.

Data validation is performed by comparison with experimental results available in literature. A comprehensive

discussion, limited to the ground or, in the luckiest cases, to the first few vibrational levels, for data here reviewed can be found in the original papers and also in the Phys4Entry database [19]. In general, satisfactory agreement is observed.

However, it should be stressed that there are issues still to be addressed, i.e. the detailed vibrational kinetics for triatomic molecules, accounting for the complex multi-mode vibrational structure and the dynamical characterization of the inter-mode coupling, the role of non-adiabatic coupling (conical intersection) among different electronic states, resulting in multi-surface dynamics, and the possible role of excited species in heavy particle collisions, not to mention the role of electronically excited states in the development of collisional-radiative models and in affecting the thermodynamic and transport properties of equilibrium plasmas [253, 254].

All these problems need attention and represent future challenges for the molecular dynamic community.

Acknowledgments

The research leading to these results has received funding from the European Community's Seventh Framework Programme (FP7/2007-2013) under grant agreement n. 242311. R Sayós and P Gamallo received partial financial support from the Spanish MINECO CTQ2014-53987-R project and from the Generalitat de Catalunya 2014SGR1582 project. M Rutigliano also received partial support from MIUR (PRIN2010ERFKXL_008). A Laganà and A Lombardi thank the VII FP (Egi-Inspire), the COST (Action CM901), the Dipartimento di Chimica, Biologia e Biotecnologie di Perugia and the 'Fondazione Cassa Risparmio Perugia (Codice Progetto: 2015.0331.021 Ricerca Scientifica e Tecnologica)'. A Lombardi gratefully acknowledges financial support from Italian MIUR (PRIN 2010-2011, grant 2010ERFKXL), and allocated computing time from the Virtual Organization COMPCHEM and the OU Supercomputing Center for Education & Research (OSCER) at the University of Oklahoma (OU).

References

[1] Park C (ed) 2012 *Nonequilibrium Hypersonic Aerothermodynamics* (New York: Wiley)
[2] Colonna G, Armenise I, Bruno D and Capitelli M 2006 *J. Thermophys. Heat Transfer* **20** 477–86
[3] Colonna G, Pietanza L D and Capitelli M 2008 *J. Thermophys. Heat Transfer* **22** 399–406
[4] Guy A, Bourdon A and Perrin M Y 2013 *Chem. Phys.* **420** 15–24
[5] Capitelli M (ed) 1986 *Nonequilibrium Vibrational Kinetics* (*Springer Series Topics in Current Physics* vol 39) (New York: Springer)
[6] Loureiro J, Guerra V, Sá P A, Pintassilgo C D and Lino da Silva M 2011 *Plasma Sources Sci. Technol.* **20** 024007
[7] Capitelli M, Celiberto R, Colonna G, Esposito F, Gorse C, Hassouni K, Laricchiuta A and Longo S 2016 *Fundamental Aspects of Plasma Chemical Physics: Kinetics* (*Springer Series on Atomic, Optical, and Plasma Physics* vol 85) (New York: Springer)
[8] Nagnibeda E and Kustova E 2009 *Non-Equilibrium Reacting Gas Flows: Kinetic Theory of Transport and Relaxation Processes* (*Springer Series on Heat and Mass Transfer*) (Berlin: Springer)
[9] Perrin M Y, Riviére P and Soufiani A 2012 *Radiation Phenomena Behind Shock Waves* (*High Temperature Phenomena in Shock Waves* vol 50) ed R Brun (New York: Springer)
[10] Surzhikov S T 2012 *J. Heat Transfer* **134** 031002–2
[11] Bultel A and Annaloro J 2013 *Plasma Sources Sci. Technol.* **22** 025008
[12] Colonna G, D'Ammando G, Pietanza L D and Capitelli M 2015 *Plasma Phys. Control. Fusion* **57** 014009
[13] D'Ammando G, Capitelli M, Esposito F, Laricchiuta A, Pietanza L D and Colonna G 2014 *Phys. Plasmas* **21** 093508
[14] Capitelli M, Colonna G, Pietanza L and D'Ammando G 2013 *Spectrochim. Acta* B **83–4** 1–13
[15] Capitelli M *et al* 2007 *Plasma Sources Sci. Technol.* **16** S30
[16] Capitelli M *et al* 2006 *Nucl. Fusion* **46** S260
[17] Armenise I and Capitelli M 2005 *Plasma Sources Sci. Technol.* **14** S9
[18] LXcat 2015 Plasma Data Exchange Project database http://fr.lxcat.net/home/
[19] 2015 Phys4Entry database http://phys4entrydb.ba.imip.cnr.it/Phys4EntryDB/
[20] 2015 STELLAR http://esther.ist.utl.pt/pages/stellar.html
[21] Colonna G and Capitelli M 2008 *J. Thermophys. Heat Transfer* **22** 414–23
[22] Capitelli M *et al* 2012 *Plasma Chem. Plasma Process.* **32** 427–50
[23] Panesi M, Jaffe R L, Schwenke D W and Magin T E 2013 *J. Chem. Phys.* **138** 044312
[24] Capitelli M, Colonna G, D'Ammando G, Laporta V and Laricchiuta A 2014 *Chem. Phys.* **438** 31–6
[25] Munafò A and Magin T E 2014 *Phys. Fluids* **26** 097102
[26] Armenise I and Esposito F 2015 *Chem. Phys.* **446** 30–46
[27] Armenise I, Esposito F and Capitelli M 2007 *Chem. Phys.* **336** 83–90
[28] Armenise I and Esposito F 2012 *Chem. Phys.* **398** 104–10 (special issue Chemical Physics of Low-Temperature Plasmas (in honour of Prof Mario Capitelli))
[29] Loureiro J, Ferreira C M, Capitelli M, Gorse C and Cacciatore M 1990 *J. Phys. D: Appl. Phys.* **23** 1371
[30] Colonna G, Laporta V, Celiberto R, Capitelli M and Tennyson J 2015 *Plasma Sources Sci. Technol.* **24** 035004
[31] Laporta V, Celiberto R and Tennyson J 2013 *Plasma Sources Sci. Technol.* **22** 025001
[32] Laporta V, Celiberto R and Wadehra J M 2012 *Plasma Sources Sci. Technol.* **21** 055018
[33] Laporta V, Cassidy C M, Tennyson J and Celiberto R 2012 *Plasma Sources Sci. Technol.* **21** 045005
[34] Laporta V, Little D A, Celiberto R and Tennyson J 2014 *Plasma Sources Sci. Technol.* **23** 065002
[35] Laporta V, Celiberto R and Tennyson J 2015 *Phys. Rev.* A **91** 012701
[36] Capitelli M and Celiberto R 1998 *Novel Aspects of Electron-Molecule Collisions* ed K H Becker (Singapore: World Scientific) pp 283–323
[37] Laricchiuta A, Celiberto R and Capitelli M 2000 *Chem. Phys. Lett.* **329** 526–32
[38] Celiberto R, Janev R, Laricchiuta A, Capitelli M, Wadehra J and Atems D 2001 *At. Data Nucl. Data Tables* **77** 161–213
[39] Kosarim A, Smirnov B, Capitelli M, Celiberto R, Petrella G and Laricchiuta A 2005 *Chem. Phys. Lett.* **414** 215–21
[40] Laricchiuta A, Capitelli M, Celiberto R and Colonna G 2006 *37th AIAA Plasmadynamics and Lasers Conf. (San Francisco, CA, USA, 5–8 June 2006)* AIAA-2006-2898
[41] Kosarim A, Smirnov B, Capitelli M, Celiberto R, Laricchiuta A and Paniccia F 2006 *Chem. Phys. Lett.* **422** 513–7

[42] Esposito F, Armenise I and Capitelli M 2006 *Chem. Phys.* **331** 1–8
[43] Caridade P J S B, Galvão B R L and Varandas A J C 2010 *J. Phys. Chemi.* A **114** 6063–70
[44] Akpinar S, Armenise I, Defazio P, Esposito F, Gamallo P, Petrongolo C and Sayós R 2012 *Chem. Phys.* **398** 81–9
[45] Laganà A and Garcia E 2015 *VIRT&L-COMM* **5** 5–2014.10 (available at: http://www.hpc.unipg.it/ojs/index.php/virtlcomm/article/view/18)
[46] Laganà A, de Aspuru G O and Garcia E 2015 *VIRT&L-COMM* **5** 5–2014.11 (available at: http://www.hpc.unipg.it/ojs/index.php/virtlcomm/article/view/19)
[47] Laganà A, Garcia E and Martínez T 2014 *VIRT&L-COMM* **5** 5–2014.12 (available at: http://www.hpc.unipg.it/ojs/index.php/virtlcomm/article/view/20)
[48] Andrienko D and Boyd I D 2015 *Chem. Phys.* **459** 1–13
[49] Jaffe R, Schwenke D and Chaban G 2009 *AIAA-Paper 2009-1569*
[50] Bose D and Candler G V 1997 *J. Chem. Phys.* **107** 6136–45
[51] Bose D and Candler G V 1996 *J. Chem. Phys.* **104** 2825–33
[52] Billing G 1986 *Nonequilibrium Vibrational Kinetics* vol 39, ed M Capitelli (New York: Springer)
[53] Capitelli M, Gorse C and Billing G 1980 *Chem. Phys.* **52** 299–304
[54] Cacciatore M, Kurnosov A and Napartovich A 2005 *J. Chem. Phys.* **123** 174315
[55] Kurnosov A, Cacciatore M, Laganà A, Pirani F, Bartolomei M and Garcia E 2014 *J. Comput. Chem.* **35** 722–36
[56] Kurnosov A K, Napartovich A P, Shnyrev S L and Cacciatore M 2010 *Plasma Sources Sci. Technol.* **19** 045015
[57] Garcia E, Martínez T and Laganà A 2015 *Chem. Phys. Lett.* **620** 103–8
[58] Adamovich I V, MacHeret S O, Rich J W and Treanor C E 1998 *J. Thermophys. Heat Transfer* **12** 57–65
[59] Lino da Silva M, Guerra V and Loureiro J 2009 *Plasma Sources Sci. Technol.* **18** 034023
[60] Lino da Silva M, Loureiro J and Guerra V 2012 *Chem. Phys. Lett.* **531** 28–33
[61] Coletti C and Billing G 2002 *Chem. Phys. Lett.* **356** 14–22
[62] Bender J D, Valentini P, Nompelis I, Paukku Y, Varga Z, Truhlar D G, Schwartzentruber T and Candler G V 2015 *J. Chem. Phys.* **143** 054304
[63] Valentini P, Schwartzentruber T E, Bender J D, Nompelis I and Candler G V 2015 *Phys. Fluids* **27** 086102
[64] Esposito F and Capitelli M 2009 *J. Phys. Chem.* A **113** 15307–14
[65] Forrey R C 2013 *Phys. Rev.* A **88** 052709
[66] Muiño R D and Busnengo H F (ed) 2013 *Dynamics of Gas-Surface Interactions: Atomic-Level Understanding of Scattering Processes at Surfaces* (*Springer Series in Surface Science* vol 50) (New York: Springer)
[67] Cacciatore M and Rutigliano M 2009 *Plasma Sources Sci. Technol.* **18** 023002
[68] Armenise I, Barbato M, Capitelli M and Kustova E 2006 *J. Thermophys. Heat Transfer* **20** 465–76
[69] Armenise I, Rutigliano M, Cacciatore M and Capitelli M 2011 *J. Thermophys. Heat Transfer* **25** 627–32
[70] Armenise I and Kustova E V 2014 *Chem. Phys.* **428** 90–104
[71] Molinari E and Tomellini M 2006 *Catalysis Today* **116** 30–7
[72] Arasa C, Morón V, Busnengo H F and Sayós R 2009 *Surf. Sci.* **603** 2742–51
[73] Morón V, Gamallo P, Martin-Gondre L, Crespos C, Larregaray P and Sayós R 2011 *Phys. Chem. Chem. Phys.* **13** 17494
[74] Morón V, Martin-Gondre L, Gamallo P and Sayós R 2012 *J. Phys. Chem.* C **116** 13092–103
[75] Bedra L, Rutigliano M, Balat-Pichelin M and Cacciatore M 2006 *Langmuir* **22** 7208–16
[76] Cacciatore M, Rutigliano M and Billing G D 1999 *J. Thermophys. Heat Transfer* **13** 195–203
[77] Cacciatore M 1999 *Pure Appl. Chem.* **71** 1809–17
[78] Rutigliano M, Zazza C, Sanna N, Pieretti A, Mancini G, Barone V and Cacciatore M 2009 *J. Phys. Chem.* A **113** 15366–75
[79] Zazza C, Rutigliano M, Sanna N, Barone V and Cacciatore M 2012 *J. Phys. Chem.* A **116** 1975–83
[80] Rutigliano M, Pieretti A, Cacciatore M, Sanna N and Barone V 2006 *Surf. Sci.* **600** 4239–46
[81] Rutigliano M, Gamallo P, Sayós R, Orlandini S and Cacciatore M 2014 *Plasma Sources Sci. Technol.* **23** 045016
[82] Rutigliano M and Cacciatore M 2016 *J. Thermophys. Heat Transfer* **30** 247–50
[83] Celiberto R, Janev R K, Wadehra J M and Laricchiuta A 2008 *Phys. Rev.* A **77** 012714
[84] Celiberto R, Janev R K, Wadehra J M and Laricchiuta A 2009 *Phys. Rev.* A **80** 012712
[85] Capitelli M *et al* 2010 *J. Phys. B: At. Mol. Opt. Phys.* **43** 144025
[86] Celiberto R, Janev R K, Wadehra J M and Laricchiuta A 2011 *Phys. Rev.* A **84** 012707
[87] Celiberto R, Janev R K, Laporta V, Tennyson J and Wadehra J M 2013 *Phys. Rev.* A **88** 062701
[88] Armenise I and Kustova E 2013 *Chem. Phys.* **415** 269–81
[89] Kozàk T and Bogaerts A 2014 *Plasma Sources Sci. Technol.* **23** 045004
[90] Taylan O and Berberoglu H 2015 *Plasma Sources Sci. Technol.* **24** 015006
[91] Celiberto R, Laporta V, Laricchiuta A, Wadehra J and Tennyson J 2014 *Open Plasma Phys. J.* **7** 33–47
[92] Lombardi A, Faginas-Lago N, Pacifici L and Costantini A 2013 *J. Phys. Chem.* A **117** 11430–40
[93] Gamallo P, Prats H and Sayós R 2014 *J. Mol. Model.* **20** 2160
[94] Laganà A, Lombardi A, Pirani F, Gamallo P, Sayós R, Armenise I, Cacciatore M, Esposito F and Rutigliano M 2014 *Open Plasma Phys. J.* **7** 48–59
[95] Pietanza L D, Colonna G, D'Ammando G, Laricchiuta A and Capitelli M 2015 *Plasma Sources Sci. Technol.* **24** 042002
[96] Gryziński M 1965 *Phys. Rev.* **138** A336–58
[97] Chung S and Lin C C 1972 *Phys. Rev.* A **6** 988–1002
[98] Hazi A U 1981 *Phys. Rev.* A **23** 2232–40
[99] Redmon M J, Garrett B C, Redmon L T and McCurdy C W 1985 *Phys. Rev.* A **32**(6) 3354–65
[100] Celiberto R and Rescigno T N 1993 *Phys. Rev.* A **47** 1939–45
[101] Kim Y K 2007 *J. Chem. Phys.* **126** 064305
[102] Adamson S, Astapenko V, Deminskii M, Eletskii A, Potapkin B, Sukhanov L and Zaitsevskii A 2007 *Chem. Phys. Lett.* **436** 308–13
[103] Kim Y K and Rudd M E 1994 *Phys. Rev.* A **50** 3954–67
[104] Nishimura H and Danjo A 1986 *J. Phys. Soc. Japan* **55** 3031–6
[105] Khakoo M A, Trajmar S, McAdams R and Shyn T W 1987 *Phys. Rev.* A **35** 2832–7
[106] Khakoo M A and Segura J 1994 *J. Phys. B: At. Mol. Opt. Phys.* **27** 2355
[107] Stibbe D T and Tennyson J 1998 *New J. Phys.* **1** 2
[108] Trevisan C S and Tennyson J 2002 *Plasma Phys. Control. Fusion* **44** 1263
[109] Rescigno T N and Schneider B I 1988 *J. Phys. B: At. Mol. Opt. Phys.* **21** L691
[110] Celiberto R, Capitelli M and Laricchiuta A 2002 *Phys. Scr.* **2002** 32
[111] Liu X, Shemansky D E, Johnson P V, Malone C P, Khakoo M A and Kanik I 2012 *J. Phys. B: At. Mol. Opt. Phys.* **45** 015201
[112] Laricchiuta A, Celiberto R and Janev R K 2004 *Phys. Rev.* A **69** 022706
[113] Wünderlich D 2011 *Chem. Phys.* **390** 75–82
[114] Celiberto R, Baluja K L, Janev R K and Laporta V 2016 *Plasma Phys. Control. Fusion* **58** 014024
[115] Cosby P C 1993 *J. Chem. Phys.* **98** 9544–53

[116] Capitelli M, Celiberto R, Eletskii A and Laricchiuta A 2001 *At. Plasma Mater. Interact. Data Fusion* **9** 47–64
[117] Wakiya K 1978 *J. Phys. B: At. Mol. Phys.* **11** 3913
[118] Suzuki D, Kato H, Ohkawa M, Anzai K, Tanaka H, Limõ-Vieira P, Campbell L and Brunger M J 2011 *J. Chem. Phys.* **134** 064311
[119] Stahel D, Leoni M and Dressler K 1983 *J. Chem. Phys.* **79** 2541–58
[120] Spelsberg D and Meyer W 2001 *J. Chem. Phys.* **115** 6438–49
[121] Gibson S T and Lewis B R 1996 *J. Electron Spectrosc. Relat. Phenom.* **80** 9–12
[122] Lewis B R, England J P, Gibson S T, Brunger M J and Allan M 2001 *Phys. Rev.* A **63** 022707
[123] Khakoo M A, Malone C P, Johnson P V, Lewis B R, Laher R, Wang S, Swaminathan V, Nuyujukian D and Kanik I 2008 *Phys. Rev.* A **77** 012704
[124] Malone C P, Johnson P V, Liu X, Ajdari B, Kanik I and Khakoo M A 2012 *Phys. Rev.* A **85** 062704
[125] Straub H C, Renault P, Lindsay B G, Smith K A and Stebbings R F 1996 *Phys. Rev.* A **54** 2146–53
[126] Krishnakumar E and Srivastava S K 1990 *J. Phys. B: At. Mol. Opt. Phys.* **23** 1893
[127] Shemansky D E and Liu X 2005 *J. Geophys. Res.: Space Phys.* **110** A07307
[128] Cacciatore M, Capitelli M and Gorse C 1982 *Chem. Phys.* **66** 141–51
[129] Van Zyl B and Pendleton W 1995 *J. Geophys. Res.: Space Phys.* **100** 23755–62
[130] Doering J P and Yang J 1997 *J. Geophys. Res.: Space Phys.* **102** 9691–6
[131] Stibbe D T and Tennyson J 1998 *J. Phys. B: At. Mol. Opt. Phys.* **31** 815–44
[132] Allan M 1985 *J. Phys. B: At. Mol. Opt. Phys.* **18** 4511
[133] Noble C J, Higgins K, Wöste G, Duddy P, Burke P G, Teubner P J O, Middleton A G and Brunger M J 1996 *Phys. Rev. Lett.* **76** 3534–7
[134] Allan M 1995 *J. Phys. B: At. Mol. Opt. Phys.* **28** 5163
[135] Wong S F, Boness M J W and Schulz G J 1973 *Phys. Rev. Lett.* **31** 969–72
[136] Laporta V, Celiberto R and Tennyson J 2014 *AIP Conf. Proc.* **1628** 939–42
[137] Trevisan C S, Houfek K, Zhang Z, Orel A E, McCurdy C W and Rescigno T N 2005 *Phys. Rev.* A **71** 052714
[138] Allan M 2005 *J. Phys. B: At. Mol. Opt. Phys.* **38** 603
[139] Allan M 2004 *J. Phys. B: At. Mol. Opt. Phys.* **37** L359–63
[140] Nandi D, Prabhudesai V S, Nestmann B M and Krishnakumar E 2011 *Phys. Chem. Chem. Phys.* **13** 1542–51
[141] Laporta V, Celiberto R and Tennyson J 2016 *Plasma Sources Sci. Technol.* **25** 01LT04
[142] Allan M 2010 *Phys. Rev.* A **81** 042706
[143] Bardsley J N and Wadehra J M 1979 *Phys. Rev.* A **20** 1398–405
[144] Horáček J, Čížek M, Houfek K, Kolorenč P and Domcke W 2006 *Phys. Rev.* A **73** 022701
[145] Schulz G J 1973 *Rev. Mod. Phys.* **45** 423–86
[146] Wadehra J M and Bardsley J N 1978 *Phys. Rev. Lett.* **41** 1795–8
[147] Wadehra J M 1979 *Appl. Phys. Lett.* **35** 917
[148] Atems D E and Wadehra J M 1990 *Phys. Rev.* A **42** 5201
[149] Horáč J, Čížek M, Houfek K, Kolorenč P and Domcke W 2004 *Phys. Rev.* A **70** 052712
[150] Atems D E and Wadehra J M 1993 *J. Phys. B: At. Mol. Opt. Phys.* **26** L759
[151] Celiberto R, Janev R, Wadehra J and Tennyson J 2012 *Chem. Phys.* **398** (Special Issue Chemical Physics of Low-Temperature Plasmas (in honour of Prof Mario Capitelli)) 206–13
[152] Comer J and Read F H 1971 *J. Phys.* B **4** 368
[153] Houfek K, Rescigno T N and McCurdy C W 2006 *Phys. Rev.* A **73** 032721
[154] Huo W M, Gibson T L, Lima M A P and McKoy V 1987 *Phys. Rev.* A **36** 1632–41
[155] Tennyson J 2010 *Phys. Rep.* **491** 29–76
[156] Domcke W 1991 *Phys. Rep.* **208** 97–188
[157] Burke P G 2011 *R-Matrix Theory of Atomic Collisions: Application to Atomic, Molecular and Optical Processes* (New York: Springer)
[158] Tennyson J 1996 *J. Phys. B: At. Mol. Opt. Phys.* **29** 1817–28
[159] Tennyson J and Noble C J 1984 *Comput. Phys. Commun.* **33** 421–4
[160] Stibbe D T and Tennyson J 1996 *J. Phys. B: At. Mol. Opt. Phys.* **29** 4267–83
[161] Berman M, Estrada H, Cederbaum L S and Domcke W 1983 *Phys. Rev.* A **28** 1363–81
[162] Mündel C, Berman M and Domcke W 1985 *Phys. Rev.* A **32** 181
[163] Nestmann B M, Kumar S V K and Peyerimhoff S D 2005 *Phys. Rev.* A **71** 012705
[164] Little D A and Tennyson J 2014 *J. Phys. B: At. Mol. Opt. Phys.* **47** 105204
[165] Little D. A and Tennyson J 2013 *J. Phys. B: At. Mol. Opt. Phys.* **46** 145102
[166] Werner H J, Knowles P J, Knizia G, Manby F R and Schütz M 2012 *WIREs Comput. Mol. Sci.* **2** 242–53
[167] Spence D and Burrow P D 1979 *J. Phys B: At. Mol. Phys.* **12** L179
[168] Huetz A, Gresteau F, Hall R I and Mazeau J 1980 *J. Chem. Phys.* **72** 5297–304
[169] Huetz A, Gresteau F and Mazeau J 1980 *J. Phys. B: At. Mol. Phys.* **13** 3275
[170] Fabrikant I I, Wadhera J M and Xu Y 2002 *Phys. Scr.* **2002** 45
[171] Bieniek R J and Dalgarno A 1979 *Astrophys. J.* **228** 635
[172] Kreckel H, Bruhns H, Čížek M, Glover S C O, Miller K A, Urbain X and Savin D W 2010 *Science* **329** 69
[173] Sheehan C H and St-Maurice J P 2004 *J. Geophys. Res.* **109** A03302
[174] Little D A, Chakrabarti K, Mezei J Z, Schneider I F and Tennyson J 2014 *Phys. Rev.* A **90** 052705
[175] Larsson M and Orel A E 2008 *Dissociative Recombination of Molecular Ions* (Cambridge: Cambridge University Press)
[176] Schneider I F, Dulieu O and Robert J (ed) 2013 *Proc. of Ninth Int. Conf. on Dissociative Recombination: Theory, Experiment and Applications (Paris, France)*
[177] Hutson J M and Green S 1994 MOLSCAT computer code version 14, Collaborative. Computational Project No. 6 of the Engineering and Physical Sciences Research. Council (UK).
[178] Hase W L *et al* 1996 *J. Quantum Chem. Program Exch. Bull.* **16** 671
[179] Billing G 1984 *Comput. Phys. Rep.* **1** 239–96
[180] De Fazio D 2014 *Phys. Chem. Chem. Phys.* **16** 11662–72
[181] Gervasi O, Manuali C, Laganà A and Costantini A 2009 *Chemistry and Material Science Applications on Grid Infrastructures* (*ICTP Lecture Notes* vol 24) (Trieste: ICTP) p 63
[182] Maitland G C, Rigby M, Smith E B and Wakeham W A 1987 *Intermolecular Forces* (Oxford: Clarendon)
[183] Nasri S, Ajili V, Jaidane N, Kalugina Y N, Halvick P, Stoecklin T and Hochlaf H 2015 *J. Chem. Phys.* **142** 174301
[184] Bartolomei M, Pirani F, Laganà A and Lombardi A 2012 *J. Comput. Chem.* **33** 1806–19
[185] Laganà A and Riganelli A 2000 *Fitting Potential Energy Surfaces in Reaction and Molecular Dynamics* (*Lecture Notes in Chemistry* vol 14) ed G C Schatz (New York: Springer)
[186] Garcia E and Laganà A 1985 *Mol. Phys.* **56** 629–39
[187] Garcia E and Laganà A 1985 *Mol. Phys.* **56** 621–7
[188] Garcia E, Sanchez C, Rodriguez A and Laganà A 2006 *Int. J. Quantum Chem.* **106** 623–30

[189] Rodriguez A, Garcia E, Hernandez M and Laganà A 2012 *Chem. Phys. lett.* **360** 304–12
[190] Garcia E, Kurnosov A, Laganà A, Pirani F, Bartolomei M and Cacciatore M 2016 *J. Phys. Chem.* B **120** 1476–85
[191] Lombardi A, Faginas-Lago N, Pacifici L and Grossi G 2015 *J. Chem. Phys.* **143** 034307
[192] Lombardi A, Faginas-Lago N and Laganà A 2014 *Grid Calculation Tools for Massive Applications of Collision Dynamics Simulations: Carbon Dioxide Energy Transfer* (*Computational Science and Its Applications—ICCSA 2014* vol 8579) (New York: Springer)
[193] Lombardi A, Laganà A, Pirani F, Palazzetti F and Faginas-Lago N 2013 *Carbon Oxides in Gas Flows and Earth and Planetary Atmospheres: State-to-State Simulations of Energy Transfer and Dissociation Reactions* (*Computational Science and Its Applications—ICCSA 2013*) (New York: Springer)
[194] Billing G D 1976 *J. Chem. Phys.* **65**
[195] Cacciatore M, Kurnosov A, Napartovich A and Shnyrev A 2004 *J. Phys.* **37** 3379
[196] Kurnosov A, Napartovich A, Shnyrev S and Cacciatore M 2007 *J. Phys. Chem.* **111** 7057
[197] Park H and Slanger T G 1994 *J. Chem. Phys.* **100** 287–300
[198] Billing G D 1994 *Chem. Phys.* **179** 463–7
[199] Wang D, Stallcop J R, Huo W M, Dateo C E, Schwenke D W and Partridge H 2003 *J. Chem. Phys.* **118** 2186–9
[200] Rampino S, Skouteris D, Laganà A, Garcia E and Saracibar A 2009 *Phys. Chem. Chem. Phys.* **11** 1752
[201] Faginas N, Naga F H L and Laganà A 2008 *Chem. Phys. Lett.* **464** 249–55
[202] Schwartz R N, Slawsky Z I and Herzfeld K F 1952 *J. Chem. Phys.* **20** 1591–9
[203] Rapp D and Kassal T 1969 *Chem. Rev.* **69** 61–102
[204] Adamovich I V 2014 *Phys. Fluids* **26** 046102
[205] Lino da Silva M, Guerra V, Loureiro J and Sá P A 2008 *Chem. Phys.* **348** 187–94
[206] Parker G A and Pack R T 1978 *J. Chem. Phys.* **68** 1585
[207] Esposito F, Coppola C M and De Fazio D 2015 *J. Phys. Chem.* A **119** 12615–26
[208] Laganà A, Garcia E and Ciccarelli L 1987 *J. Phys. Chem.* **91** 312–4
[209] Laganà A and Garcia E 1994 *J. Phys. Chem.* **98** 502–7
[210] Armenise I, Capitelli M and Gorse C 1996 *J. Thermophys. Heat Transfer* **10** 397
[211] Armenise I, Capitelli M, Kustova E and Nagnibeda E 1999 *J. Thermophys. Heat Transfer* **13** 210–8
[212] Esposito F, Armenise I and Capitelli M 2006 *Europhys. Conf. Abstr.* **30G** 173 (*18th Europhysics Conf. on the Atomic and Molecular Physics of Ionized Gases)*
[213] Laganà A, de Aspuru G O and Garcia E 1994 *6th Joint Thermophysics and Heat Transfer Conf.*
[214] Laganà A, Ochoa De Aspuru G and Garcia E 1996 Dipartimento di Chimica, Università di Perugia Perugia, Italy
[215] Esposito F and Capitelli M 2006 *Chem. Phys. Lett.* **418** 581–5
[216] Bruno D, Capitelli M, Esposito F, Longo S and Minelli P 2002 *Chem. Phys. Lett.* **360** 31–7
[217] Esposito F, Capitelli M and Gorse C 2000 *Chem. Phys.* **257** 193–202
[218] Galvão B R L and Varandas A J C 2009 *J. Phys. Chem.* **113** 14424–30
[219] Ernesto G, Amaia S, Gómez-Carrasco S and Laganà A 2008 *Phys. Chem. Chem. Phys.* **10** 2552–8
[220] Esposito F and Capitelli M 2002 *Chem. Phys. Lett.* **364** 180–7
[221] Li Y, Sun Z, Jiang B, Xie D, Dawes R and Guo H 2014 *J. Chem. Phys.* **141** 081102
[222] Varandas A and Pais A 1988 *Mol. Phys.* **65** 843–60
[223] Esposito F and Capitelli M 2007 *Chem. Phys. Lett.* **443** 222–6
[224] Esposito F, Armenise I, Capitta G and Capitelli M 2008 *Chem. Phys.* **351** 91–8
[225] Ivanov M V, Schinke R and Mcbane G C 2007 *Mol. Phys.* **105** 1183–91
[226] Miller W H 1970 *Chem. Phys. Lett.* **7** 431
[227] Kustova E V 2001 *Chem. Phys.* **270** 177–95
[228] Capitelli M, Colonna G and Esposito F 2004 *J. Phys. Chem.* A **108** 8930–4
[229] Armenise I, Reynier P and Kustova E 2015 *J. Thermophys. Heat Transfer* at press
[230] Lowke J J, Phelps A V and Irwin B W 1973 *J. Appl. Phys.* **44** 4664–71
[231] Phelps A V 2015 at LXcat http://nl.lxcat.net/data/set_type.php
[232] Pietanza L D, Colonna G, D'Ammando G, Laricchiuta A and Capitelli M 2016 *Phys. Plasmas* **23** 013515
[233] Pietanza L D, Colonna G, D'Ammando G, Laricchiuta A and Capitelli M 2016 *Chem. Phys.* **468** 44–52
[234] Fridman A 2012 *Plasma Chemistry* (Cambridge: Cambridge University Press)
[235] Rescigno T N, Isaacs W A, Orel A E, Meyer H D and McCurdy C W 2002 *Phys. Rev.* A **65** 032716
[236] Kustova E V, Nagnibeda E A and Armenise I 2014 *Open Plasma Phys. J.* **7** 76–87
[237] Kozàk T and Bogaerts A 2015 *Plasma Sources Sci. Technol.* **24** 015024
[238] Laub B and Venkatapathy E 2003 *Proc. of the Int. Workshop on Planetary Entry and Descent Trajectory Analysis and Science (Lisbon, Portugal)*
[239] Bertin J J and Cummings R M 2003 *Prog. Aerosp. Sci.* **39** 511–6
[240] Fletcher K (ed) 2006 *Proc. of the 5th Workshop of Thermal Protection Systems and Hot Structures (Noordwijk, The Netherlands)* ESA SP-631
[241] Armenise I, Capitelli M, Gorse C, Cacciatore M and Rutigliano M 2000 *J. Spacecr. Rockets* **37** 318–23
[242] Billing G D 2000 *Dynamics of Molecule Surface Interaction* (New York: Wiley)
[243] Cacciatore M and Billing G D 1990 *Surf. Sci.* **232** 35–50
[244] Arasa C, Busnengo H F, Salin A and Sayós R 2008 *Surf. Sci.* **602** 975–85
[245] Sayós R, Morón V, Arasa C and Busnengo H F 2009 *Proc. of the 6th European Symp. on Aerothermodynamics for Space Vehicles (Versailles, France)* ESA SP-659
[246] Bedra L and Balat-Pichelin M 2005 *Aerosp. Sci. Technol.* **9** 318–28
[247] Berkut V D, Doroshenko V M, Kovtun V V, Koudryavtsev N N, Novikov S S, Smirnov N V and Sharotovov A I 1992 *Sov. J. Chem. Phys.* **9** 2222–37
[248] Gamallo P, Rutigliano M, Orlandini S, Cacciatore M and Sayós R 2012 *AIP Conf. Proc.* **1501** 1129–36
[249] Morón V, Gamallo P and Sayós R 2011 *Theor. Chem. Acc.* **128** 683–94
[250] Morón V, Martin-Gondre L, Crespos C, Larregaray P, Gamallo P and Sayós R 2012 *Comput. Theor. Chem.* **990** 132–43 (special issue Chemical reactivity, from accurate theories to simple models, in honor of Prof Jean-Claude Rayez)
[251] Morón V, Martin-Gondre L, Gamallo P and Sayós R 2012 *J. Phys. Chem.* C **116** 21482–8
[252] Sepka S, Chen Y K, Marschall J and Copeland R A 2000 *J. Thermophys. Heat Transfer* **14** 45–52
[253] Capitelli M, Colonna G and D'Angola A 2012 *Fundamental Aspects of Plasma Chemical Physics: Thermodynamics* (*Springer Series on Atomic, Optical, and Plasma Physics* vol 66) (New York: Springer)
[254] Capitelli M, Bruno D and Laricchiuta A 2013 *Fundamental Aspects of Plasma Chemical Physics: Transport* (*Springer Series on Atomic, Optical, and Plasma Physics* vol 74) (New York: Springer)